energy&fuels

pubs.acs.org/EF Review

One Step Methanol-Mediated CO_2 Conversion to Gasoline: Comprehensive Review and Critical Outlook

Published as part of Energy & Fuels special issue "2024 Energy and Fuels Rising Stars".

Foteini Lappa, Ibrahim Khalil, Alejandro Morales, Grégoire Léonard,* and Michiel Dusselier*

Cite This: *Energy Fuels* 2024, 38, 18265−18291 Read Online

ABSTRACT: Decreasing our demand for fossil feedstock is one of the best ways to support the energy and environmental transitions that are needed for our society. CO_2 utilization and, more specifically, CO_2 conversion to hydrocarbons are an attractive route to reduce CO_2 emissions and to obtain carbon-neutral fuels and chemicals that are conventionally produced from fossil fuels. One way to achieve that is through the conversion of CO_2 to methanol, followed by methanol conversion to hydrocarbons. So far, these processes have mainly been studied as separate steps, and one view is to sequentially operate them. However, it is possible to perform it in one step, in tandem catalysis. Such catalysts are usually an oxide for the first reaction combined with an acidic zeolite that catalyzes the second reaction. Many catalysts have been researched for the two separate steps but only a few have been studied for the tandem when the gasoline range is the target. Among the oxides, ZnZrOx and In_2O_3 dominate the art, while more metallic InCo also has its merits. These lead to interesting selectivities and yields when combined with a zeolite (usually ZSM-5). A clear understanding of the mechanism behind these systems has not been reached; yet, we deliver a summary of the achieved mechanistic results and offer insights for further studies. While parameters such as bed configuration or amount proximity have been studied, more research is needed, especially when looking at the complex kinetics. This "direct CO_2 to gasoline range hydrocarbons" (including aromatics) review aims to connect dots while highlighting the aspects that still need a deeper understanding, and it also pinpoints practical insights and perspectives.

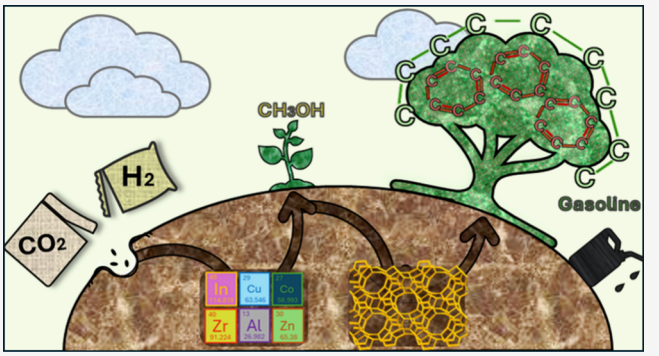

1. INTRODUCTION

Greenhouse gas (GHG) emissions are major contributors to climate change,[1] and carbon dioxide (CO_2), together with methane (CH_4), constitutes the most emitted GHG. The low lifetime of CH_4 (11−13 years) and its oxidation to CO_2 in the troposphere, together with the higher magnitude of CO_2 emissions (77% of GHG emissions), puts the focus of the emission policies on CO_2.[2,3] The development of technologies that will not only capture the produced CO_2 but also store it (carbon capture and storage, CCS) and/or use it (carbon capture and utilization, CCU) in alternative and profitable ways is essential in order to keep the temperature rise and future unpredictable climate consequences at bay.[4−6] Appealing CO_2 valorization technologies allow high-value products such as chemicals or high-volume products, including fuels, to be produced with fewer carbon emissions (or even negative ones), compared to the conventional production from gas-, oil-, and coal-based fossil fuels.[7] Multiple technologies have already been developed and can be separated into four big groups (although more could be considered);[8] the direct use of CO_2 (for example in food industry), biological fixation, mineralization, and catalytic conversion—for instance hydrogenation of CO_2 to methanol or dimethyl ether (DME).[9]

Some of these technologies are already advanced to a level at which they are either industrialized or at least ready to be scaled-up. More specifically some of the direct use and mineralization technologies are already developed at a high technology readiness level (TRL), while for certain catalytic conversions technological barriers still remain.[9] This review focuses on the catalytic conversion section and more specifically zooms in on the catalytic CO_2 to hydrocarbon hydrogenation through methanol over the competing reactions that can take place such as the methanation reaction and the reverse water−gas shift (rWGS) followed by the Fischer−

Received: June 21, 2024
Revised: August 31, 2024
Accepted: September 4, 2024
Published: September 20, 2024

https://doi.org/10.1021/acs.energyfuels.4c03013
Energy Fuels 2024, 38, 18265−18291

Tropsch synthesis (FTS) reaction (Figure 1). Thermal catalysis is an interesting method that belongs to the

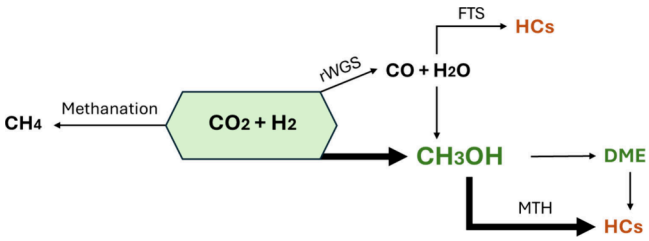

Figure 1. Zooming on catalytic CO_2 hydrogenation, pathways, and main products (rWGS = reverse water−gas shift reaction; FTS = Fischer−Tropsch synthesis reaction; MTH = methanol to hydrocarbons reaction; HCs = hydrocarbons; DME = dimethyl ether). Adapted with permission from ref 10. Copyright 2021 Elsevier.

conversion category. It is quite maturely developed (very much so for classic oil and gas feedstocks; less so for CO_2), often under high pressures and temperatures, and shows possibilities of relatively high efficiency (depending on the reaction and the system) in both space and time, but other methods such as electrocatalysis, photocatalysis, or biocatalysis are also gaining attention.[11]

It is essential to mention the importance of hydrogen as a second feedstock for this reaction. Conventionally, hydrogen is produced from fossil fuels in processes that emit huge amounts of CO_2, but more sustainable and renewable methods of producing this energy carrier have been developed.[12] Many definitions (or labels) can be used to describe hydrogen depending on the production process and its potential carbon footprint or relative CO_2 emissions (e.g., five categories in Figure 2).

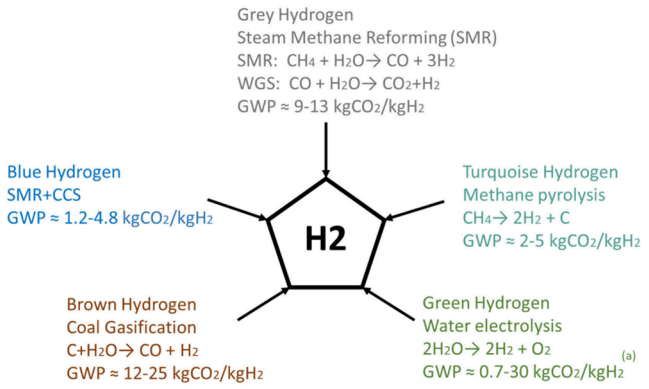

Figure 2. Hydrogen (H_2) production categories based on the used production method and its carbon footprint (global-warming potential, GWP). The CO_2 intensity is given in a range depending on calculation or technological alternatives.[13−18] (a) Highly dependent on the source and thus carbon intensity of the used electricity.

The conventional process of hydrogen production is through steam methane re-forming (SMR) followed by the water−gas shift (WGS) reaction, resulting in what is labeled Gray hydrogen.[19,20] This process is connected with large amounts of CO_2 production and energy consumption, mainly due to the highly endothermic SMR step. Consequently, when combined with CCS technologies, hydrogen could be labeled "blue", since this process could have lower carbon footprints.[21] If hydrogen is produced from coal gasification, it is labeled brown.[19,22,23] Turquoise hydrogen is produced from the pyrolysis of methane leading with no coproduction of carbon oxides but only the value-added pure carbon.[20] This solid carbon byproduct can be produced in different forms including carbon black, graphite, and nanotubes or fibers, of use in a.o. tire manufacturing, adsorption, and even catalysis.[13] Finally, green hydrogen is sometimes considered as a net-zero process, since it produces the hydrogen from water via electrolysis. Yet, depending on the type of the electrolyzer, the energy demand could be in a range of 4.5−7 kWh/(N m^3) of H_2 for alkaline electrolyzers, 4.5−7.5 kWh/(N m^3) of H_2 for polymer electrolyte ones, and 2.5−3.5 kWh/(N m^3) of H_2 for solid oxide electrolyzer.[15] The controversial point for this method is the source of used electricity, where, depending on the origin, the range of its carbon footprint can vary extensively. As Ji et al. and Bhandari et al. suggest in their reviews, nuclear-based electricity leads to the lowest footprint (<1 kg_{CO_2}/kg_{H_2}), wind-based electricity is at around 1 kg_{CO_2}/kg_{H_2}, followed by solar PV electrolysis and hydropowered electrolysis reaching almost a 2-fold footprint (≈2 kg_{CO_2}/kg_{H_2}).[15,16] It is important to mention that among the more potentially environmentally friendly types, only gray and green hydrogen categories are commercial (TRL = 9), while blue hydrogen remains to be implemented at the industrial scale (TRL = 8−9) and turquoise hydrogen is under research and demands further development (TRL = 3−4).[21]

The scope of this review is to study the catalytic hydrogenation of CO_2 to methanol followed by methanol to hydrocarbons reaction in one step or thus a tandem catalysis. This means coupling the reactions over either a combination of two different catalysts or a bifunctional catalyst (two different catalytic materials combined in one material or support), with a focus on gasoline-range hydrocarbons mainly in their saturated form and aromatics. Favoring CO_2 conversion while avoiding CO formation is challenging when aiming to couple the MeOH production with its further transformation into hydrocarbons (olefins, paraffins, or aromatics). The targets discussed here are in the gasoline region, and the definition of that region requires a deeper discussion, as done in Section 3. In that sense, coupling the two reactions requires a good understanding of the reactivity of the metal oxide in the CO_2 to methanol (CTM) step to help design efficient MeOH production catalysts operating at compatible temperatures. The state-of-the-art catalysts, the mechanistic aspect of the system, and the kinetics will be critically discussed.

2. CO_2 TO METHANOL PROCESS

Methanol (MeOH) can be used in a variety of applications, directly as a fuel or as a platform chemical.[24] There are many routes for methanol production such as electrochemical and thermochemical processes.[24] Among the thermochemical routes, the hydrogenation of gases, CO_2 is gaining more and more attention. The current commercial production route using syngas (mixture of CO, H_2, and a small amount of CO_2) was first patented in the early 1920s by BASF and operates at high pressures and temperatures in the presence of catalyst.[25] The production of MeOH requires concentrated sources of carbon (e.g., coal, natural gas, CO_2, etc.) in order to produce syngas which will further be converted to MeOH.[26] The global consumption of methanol in 2019 was 98.3 Mt, 65% of which is produced from natural gas re-forming to syngas followed by hydrogenation of the latter to methanol over heterogeneous

https://doi.org/10.1021/acs.energyfuels.4c03013
Energy Fuels 2024, 38, 18265−18291

Table 1. Selection of Key Catalysts for Direct CO_2 Hydrogenation to MeOH

Catalyst	Preparation method	H_2:CO_2	T (°C)	P (MPa)	GHSV (ml g_{cat}^{-1} h^{-1})	CO_2 conv (%)	CH_3OH select (%)	Ref
$Cu/ZnO/Al_2O_3$	Coprecipitation	3	230	3	2480[a]	18.3	43	53
$Cu/ZnO/Al_2O_3$	Hydrotalcite-like precursor derivation	3	250	5	18000	19.9	54.4	47
Cu-ZnO-ZrO_2	Coprecipitation	3	220	8	3300[b]	21	68	39
Au/Cu-ZnO-Al_2O_3	Coprecipitation	6	260	4	7000[b]	28	55	38
Pd/ZnO	Atomic layer deposition	3	250	4.5	15000	3.5	80	54
ZnO-ZrO_2	Coprecipitation	3	315	5	24000	10	91	43
FeZnZr-T-24h	Coprecipitation + TPABr treatment for 24 h	3	340	5	3750	13.9	54.3	44
In_2O_3/ZrO_2	Impregnation	4	300	5	16000[b]	5.2	99.8	37
Pd-In_2O_3-ZrO_2	Flame spray pyrolysis	4	280	5	48000	12	87	55
Ru/In_2O_3-ZrO_2	Deposition− precipitation	4	250	5	21000	4.6	88.2	46
In_2O_3	Calcination	3	270	4	15000	1.1	54.9	40
Pd/In_2O_3	Impregnation	4	300	5	21000	20	70	36
$Pt/film/In_2O_3$	plasma/peptide[c]	3	30	0.1	4800	37	62.6	45
Au/In_2O_3	Deposition−precipitation	4	300	5	21000	7.7	78	41
ZrO_2/Cu	Coprecipitation	3	220	3	48000	5	70	56
Pd/SiO_2	Coprecipitation	3	250	5	18000	0.05	100	57
Pd/CeO_2	Impregnation	3	200−260	3	2480[a]	2.1−5.2	92.9−84.7	58
$Cu/CeW_{0.25}O_x$	Impregnation	3	250	3.5	15000	13	87	59

[a]Calculated based on given W/F. [b]GHSV units given in (h^{-1}). [c]Cold plasma combined with peptide assembly for In.

catalyst.[26−28] Given the fact that this route is considered the conventional one, and that the syngas is produced from natural gas, studies by Rumayor and Irabien showed that it can have a footprint of a bit less than 0.6 kg_{CO_2}/kg_{MeOH}, which is low because the energy needed from the process comes from the natural gas.[29] This footprint value is also confirmed by the International Renewable Energy Agency and the Methanol Institute (0.5 kg_{CO_2}/kg_{MeOH}). Tackett et al. indicates that the value is a bit higher (at 1 kg_{CO_2}/kg_{MeOH}), while agreeing with the study from the International Renewable Energy Agency and Methanol Institute that the coal re-forming process has a footprint within the range of 2.6−3.8 kg_{CO_2}/kg_{MeOH}.[26,30] Through the last years many advances were applied that led to the possibility of working in less intense conditions and at lower costs.[25] More recently, one of the carbon utilization processes that has been widely studied is the production of MeOH from CO_2. The hydrogenation of CO_2 to MeOH is an exothermic reaction as described below:[7,24,31]

$$CO_2 + 3H_2 \leftrightarrow CH_3OH + H_2O, \quad \Delta H_{298K} = -49.5\ kJ/mol$$

Besides the importance of the footprint of feed gases, the environmental impact of the total process is of great significance, as well. Kim et al. studied the possibility of obtaining methanol from CO_2 in a carbon-neutral way. For this reason, they studied multiple cases where hydrogen is produced from coal gasification, SMR, and water electrolysis, as well as when methanol is directly produced from the electrolysis of CO_2.[32] Based on their literature study they came to the conclusion that the lower footprint for methanol production is via the water electrolysis for hydrogen production method followed by thermal catalysis according to the equation above, whereas CO_2 electrolysis also can have a low impact of 1.21 kg_{CO_2}/kg_{MeOH} even though there is a lack of literature on this process.[29,32] Since the carbon footprint for water electrolysis is highly dependent on many factors, such as the electricity source, specific assumptions need to be taken into account before demonstrating a value. In detail, given that photovoltaics are used for obtaining the energy needed and that CO_2 capture and CO_2 compression from atmospheric to working pressure are located at the same site, meaning that no transportation is needed, the carbon footprint can be calculated at 0.23 kg_{CO_2}/kg_{MeOH}.[29] Now that having a process with a potentially low environmental impact (mainly when the hydrogen fueling it has low CO_2 emissions) seems feasible, the focus can be shifted to optimizing the thermal catalysis behind it, meaning studying the kinetics and the optimum catalysts that could increase the yield and selectivity or, in other words, the volumetric productivity of the process. The direct CO_2 to methanol reaction is a rather new process that can be performed at temperatures of 200−300 °C and pressures in a range of 3−10 MPa.[33,34] A first commercial plant started operation in 2022 and is located in Anyang, China, owned by Carbon Recycling International, Shuncheng group, Shunju, Shunfeng, and MFE Shanghai, with a capacity of 110000 tons of MeOH/year.[35] Other pilot plants have been operating in different countries since 2004: e.g., the CAMERE process (Korean Institute of Science and Technology, 100 kg/day). The leading technology providers are in Iceland (CRI), Germany (Thyssenkrupp/Uhde/Swiss Liquid Future), Denmark (Haldor Topsoe), and U.K. (Johnson Matthey).[26]

2.1. Catalytic Materials for CO_2 to Methanol. Looking at syngas and mixtures of syngas and CO_2 as feedstocks, the commercially available catalytic material for MeOH production at an industrial level is $Cu/ZnO/Al_2O_3$.[31] However, this catalyst has limited activity and low selectivity, because of the parallel reverse water−gas shift (rWGS) reaction[36] leading to the formation of water as a main byproduct.[37] For CO_2, several other materials have been investigated, where some of the most important catalysts[31,33] for this reaction are presented in Table 1. The competition between the MeOH formation and the rWGS reaction is generally defined by the nature of the used metal oxides and can also be controlled by the operating temperature. The production of MeOH is thermodynamically favored when working at lower temperatures (<200 °C). Increasing the temperatures to further convert MeOH to

https://doi.org/10.1021/acs.energyfuels.4c03013
Energy Fuels 2024, 38, 18265−18291

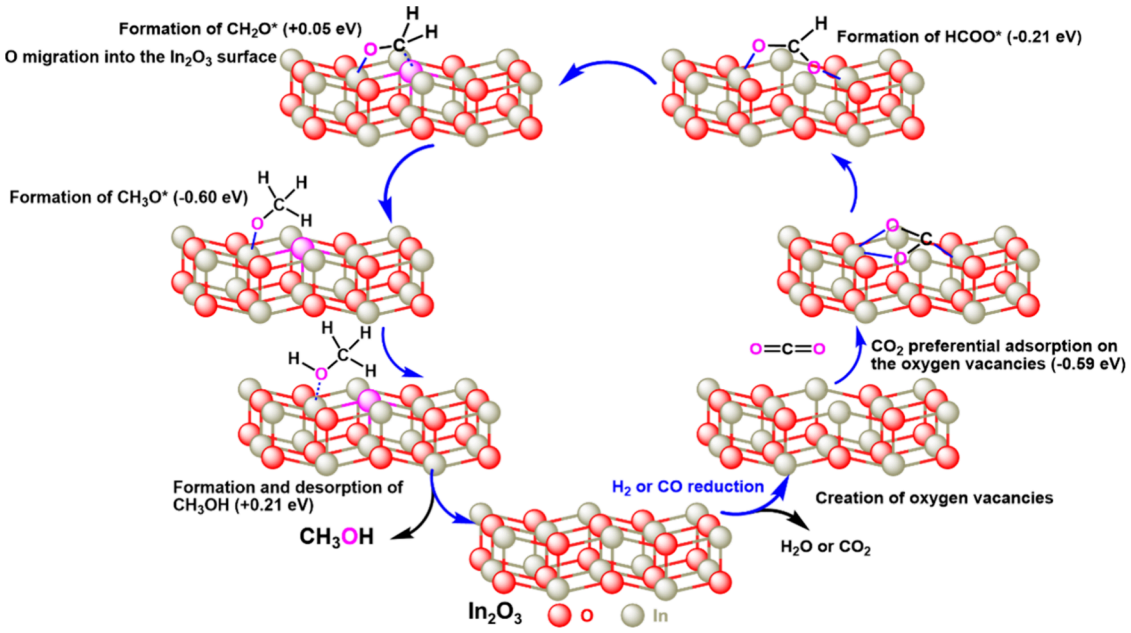

Figure 3. Demonstration of CO_2 adsorption and hydrogenation into methanol through the creation of oxygen vacancies on In_2O_3 surface. Adapted with permission from ref 61. Copyright 2013 American Chemical Society.

hydrocarbons (typically in temperatures > 300 °C) will hinder the MeOH route and the rWGS gets more prominent. Thus, catalysts operating at compatible temperatures are required. Favoring CO_2 conversion while avoiding CO formation is challenging when aiming to couple the MeOH production with its further transformation into hydrocarbons (olefins, paraffins, or aromatics), which typically occurs above 300 °C. In that sense, coupling the two reactions requires a good understanding of the reactivity of the metal oxide in the CO_2 to methanol (CTM) step to help design efficient MeOH production catalysts operating at compatible temperatures.

Among the materials presented in Table 1, some seem to show promising results. It was found by Pasupulety et al. that enhancing the conventional Cu−Zn−Al system with Au, the CO_2 conversion reached 28%.[38] Other materials that are often studied due to their catalytic properties are indium, zinc, and zirconia oxides. In 2004, Słoczynski et al. studied a system of $M/3ZnO{\cdot}ZrO_2$ where M was Cu, Ag, and Au, concluding that copper has a synergetic effect with the oxides, thus leading to the best catalytic performance with a selectivity of 68% at a conversion of 21% (see Table 1 for conditions, as without temperature (T) and gas hourly space velocity (GHSV) such numbers are meaningless).[39] About 10 years later, a different single oxide was studied for the first time, by Sun et al., In_2O_3, which exhibited high selectivity to MeOH as well (almost 55%) but suffered from a very low conversion, barely exceeding 1%.[40] In the following years, several groups have focused on improving these systems. In 2016, Perez-Ramirez and co-workers studied the In_2O_3 system and found the addition of a ZrO_2 support (In_2O_3/ZrO_2) not only increases the conversion to 5.2% but also improves the selectivity toward MeOH up to 99.8%, while maintaining its stability for about 1000 h.[37] The following year, Rui et al. showed that the addition of Pd on In_2O_3 leads to very high conversion (compared to previous works) of 20% in combination with a 70% MeOH selectivity.[36] In 2020, Rui et al. also showed that the addition of gold on In_2O_3 can increase the selectivity to MeOH to 78%; however, a lower conversion of about 7.7% was obtained.[41] It should be noted that the In_2O_3 catalyst has been proven to catalyze the reaction efficiently and has since garnered a lot of interest. Many more modifications have been studied by different groups leading to interesting results,[42] although the stability of In_2O_3 in the catalytic conditions has come under scrutiny recently. In 2017, Wang et al. reported a system of $ZnO\text{-}ZrO_2$ which exhibited a very high selectivity to MeOH (91%) and at a conversion of 10%.[43] A matrix of Fe, Zn, and Zr oxide catalysts (FeZnZr) was prepared by Wang et al., showing a higher CO selectivity than MeOH. In their effort to suppress CO production, the same group showed that a hydrothermal treatment of FeZnZr with TPABr by coprecipitation is an effective way to improve the MeOH production reaching a selectivity of the latter of 54.3% at a CO_2 conversion of 13.9% after a hydrothermal treatment for 24 h.[44] To this day, more research is being conducted toward finding more efficient catalysts in order to make the hydrogenation of CO_2 to MeOH more easily adaptable to industrial needs. On top, the exothermic nature of the reaction and the coproduction of water give additional challenges in process control and stability, respectively. An interesting entry at lower temperature is also found using $Pt/film/In_2O_3$ catalyst at 30 °C in the study of Men et al. Here, a very high conversion is reached thanks to the operation at ambient conditions that favor the thermodynamic equilibrium. However, this experiment was run using cold plasma chemistry for which process maturity is still very low, so that this kind of chemistry is not further considered in the present work.[45] More recently, Xiong et al., studied the $Ru/In_2O_3{-}ZrO_2$ catalyst showing that the combination of In_2O_3 and ZrO_2 (synthesized by coprecipitation) as support can enhance the hydrogen activation ability as well as the oxygen vacancies on the surface of the catalyst leading to higher selectivity toward methanol.[46] Lastly, in 2024, Zhang et al. studied multiple synthesis methods to increase the catalytic activity of the conventional $Cu/ZnO/Al_2O_3$, concluding that the hydrotalcite-like precursor method shows the highest methanol yield due to the high specific surface area of Cu^0 and with its small particle size and homogeneous dispersion.[47] It

https://doi.org/10.1021/acs.energyfuels.4c03013
Energy Fuels 2024, 38, 18265−18291

should be underlined that since the main focus of this review is not the CO_2 hydrogenation to MeOH but mainly the use of MeOH as an intermediate for the total CO_2 to gasoline reaction, the catalysts mentioned in Table 1 do not present a full in depth review of this reaction. There are multiple methods of synthesizing and optimizing the CO_2 to MeOH catalysts using different templates or materials, and a more detailed review can be found in the literature.[48−52]

2.2. Reaction Mechanism of the CO_2 to Methanol. The mechanism of CO_2 hydrogenation has been widely exploited and offers valuable insights into the elementary steps of the reaction, the intermediates involved, and the energy changes occurring throughout the reaction. This knowledge enabled the optimization of the reaction conditions and the better design of catalysts. In general terms, the prediction of the reaction intermediates and their formation mechanism can be done using theoretical modeling such as molecular dynamic simulations and density functional theory (DFT).[60,61] In addition, experimental mechanistic proofs can be delivered experimentally using isotopically labeled experiments (e.g., hydrogen−deuterium exchange) or operando analysis of the surface of the catalysts.[62,63] Among the operando analysis methods, DRIFTS (diffuse reflectance infrared Fourier transform spectroscopy) is the most commonly used for studying the surface properties of solid catalysts in gas-phase reactions, which explains its abundance in the reports studying the mechanism of CO_2 hydrogenation.[44,64]

In this mechanistic part of the review, we report the mechanism of hydrogenation of CO_2 to MeOH with an emphasis on the role of oxygen vacancies in the initial adsorption and CO_2 conversion. In addition, the IR vibrational bands of the different reaction intermediates (adsorbed CO_2 or carbonates, adsorbed formate species HCOO*, adsorbed formaldehyde species CH_2O*, and adsorbed methoxy species CH_3O*) will be reported and discussed.

The oxygen vacancies on the metal oxide catalyst were reported to be essential for favoring the MeOH formation from CO_2, while suppressing the rWGS.[61,65] These findings were supported by studying the energy levels of the CTM reaction steps with DFT on defective (oxygen vacancies) and perfect (inverted) In_2O_3 (110) surfaces (Figure 3). First, the defective surface was found to favor the adsorption of CO_2 with a reported adsorption energy of around −0.59 eV. However, on a perfect In_2O_3 surface, the adsorption of CO_2 was less favored (around −1.25 eV). After its adsorption, the hydrogenation of CO_2 leads to HCOO* of the COOH* species. Interestingly, the formation of the HCOO* species is slightly exothermic (−0.21 eV), which makes it thermodynamically favored over the endothermic COOH* path (+1.39 eV).[61] A similar trend was reported for a perfect In_2O_3 surface. However, the presence of oxygen vacancies was beneficial for reducing the activation energy barrier and producing the HCOO* exothermally. In the proposed mechanism, the HCOO* species are further hydrogenated by forming a new C−H bond and breaking one C−O bond to form CH_2O* and a hydroxyl (OH*) group in a thermally neutral reaction (+0.05 eV). Next, the exothermic hydrogenation of CH_2O* to CH_3O* is reported to occur at −0.60 eV, which is considered the rate-limiting step in methanol synthesis, due to its high energy barrier of 1.14 eV. Finally, methanol is obtained from the hydrogenation of the CH_3O* intermediate with an endothermic reaction of +0.21 eV.[61] Lam et al. performed in situ X-ray absorption spectroscopy to study CO_2 adsorption on ZrO_2. They demonstrated that CO_2 adsorbs preferentially on unsaturated Zr^{IV} surface sites or oxygen vacancies of a ZrO_2 catalyst.[66] In that sense, several research works were devoted to increasing the number of oxygen vacancies on metal oxide catalysts for improved methanol production. For example, the reduction of the catalyst under H_2 or CO was found to increase the number of oxygen vacancies.[67] In addition, optimizing the synthesis methods, such as the aerogel synthesized ZnO-ZrO_2 by Zhou et al., has shown superior capacity in activating CO_2 in comparison to typical ZnO-ZrO_2 catalysts prepared by coprecipitation, impregnation, and template-synthesis methods, which was correlated to its increased surface area, higher Zn/Zr ratio, and enhanced the formation of oxygen vacancies.[60]

Operando DRIFTS measurements were reported over several metal oxides, delivering a mechanistic understanding of the hydrogenation of the CO_2 over several metal oxides. The DRIFTS measurements on pure Cr_2O_3 show the formation of surface formate (HCOO*) species at 2924, 2846, 1553, and 1354 cm^{-1}, and the first two peaks were assigned to the ν(CH) stretching vibration, while the second two were attributed to (a) symmetric ν(OCO) stretching vibrations.[68] Liu et al. explored the reaction mechanism over ZnAlOx, and the time-resolved spectral acquisition showed the initial formation of HCOO* on the surface (2910, 1620, and 1375 cm^{-1}). These bands were respectively assigned to the stretching ν(CH) vibration, the asymmetric O−C−O stretching of mono- or bidentate HCOO* species, and the symmetric stretching of these same species (Supporting Information Table S1). After prolonged reaction time, the authors reported the formation of the methoxy species (CH_3O*) with peaks at 2940 and 2840 cm^{-1} assigned to their ν(CH) stretching vibrations.[69] Li et al. followed with DRIFTS the CO_2 hydrogenation over the ZnZrOx catalyst. The peaks assigned to the ν(CH) vibrations of the surface HCOO* species were observed at 2980, 2880, and 2735 cm^{-1}. In addition, distinct peaks observed at 2930 and 2824 cm^{-1} were assigned to the surface CH_3O* species (Table S1). Importantly, when cofeeding deuterated methanol (CD_3OD), in the presence of CO_2 and H_2, the chemical trapping mass spectrometry shows the mass signals for $HCOOCD_3$, CD_3CHO, and CH_3OCD_3, which are derived respectively from HCOO*, CHO*, and CH_3O* species, suggesting that these latter are the reaction intermediates for the CO_2 hydrogenation over ZnZrOx.[63]

In addition, the role of CO_x species (CO and CO_3^{-2}) on the CO_2 hydrogenation to methanol over $ZnCrO_x$ was investigated by Zhang et al. (with the goal of making aromatics on a hybrid ZnCrOx-ZSM-5 catalyst).[70] Several studies have reported a beneficial role of the presence of CO by suppressing the undesirable rWGS reaction and, more importantly, by rescuing the oxygen vacancies destroyed by CO_2 during its conversion (Figure 3).[68] Concerning the role of CO_3^{2-}, the DRIFTS measurements on the surface of $ZnCrO_x$ show surface HCOO* peaks at 2958, 2864, 2735, and 1592 cm^{-1}. In addition, the authors reported a peak at 1357 cm^{-1} which they assigned to surface CO_3^{2-}* species, and further linked its presence to the higher selectivity toward aromatics obtained in the methanol-to-aromatics (MTA) catalyzed by ZSM-5 zeolite. However, this peak can also be attributed to the ν_s(OCO) stretching of bidentate HCOO* species, typically observed in the wavenumber zone of 1351−1370 cm^{-1}.[70,71] In a more recent work, Zhou et al. followed with in situ FT-IR

https://doi.org/10.1021/acs.energyfuels.4c03013
Energy Fuels 2024, 38, 18265−18291

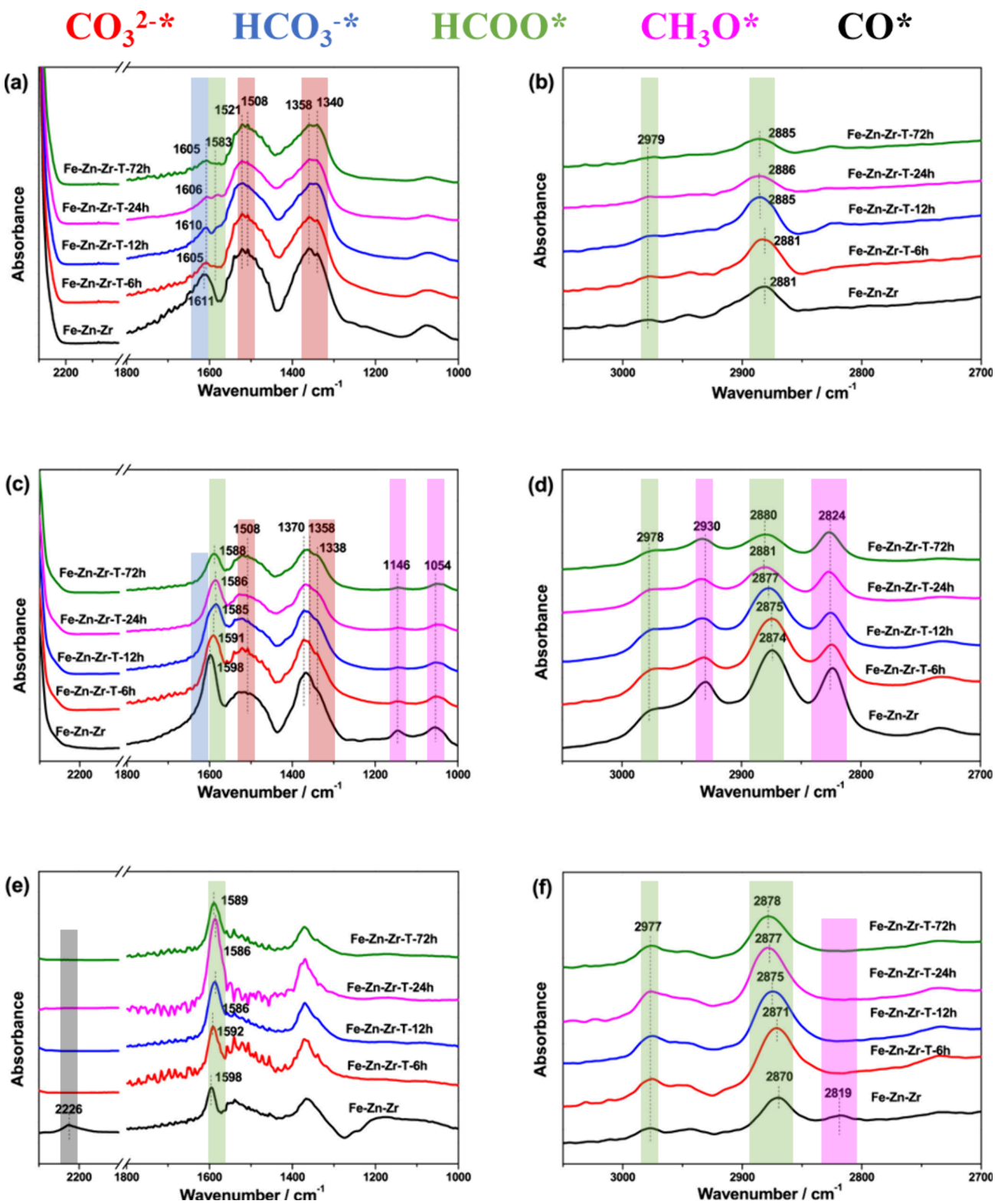

Figure 4. Reported in situ DRIFTS spectra in three different wavenumber zones: 2300−2100 cm^{-1}//1800−1000 cm^{-1} (a, c, and e) and 3050−2700 cm^{-1} (b, d, and f). The spectra show treated and untreated FeZnZr oxides during CO_2 adsorption with a highlight on the carbonates and formate species (a and b), CO_2 hydrogenation showing the formation of surface HCOO* and CH_3O* species (c and d), and the desorption of the surface species by thermal desorption under Ar flow (e and f). The time of the treatment for the different oxides is reported (from 6 to 72 h). Adapted with permission from ref44. Copyright 2021 American Chemical Society).

transmission the adsorption of pure CO_2 at 340 °C on an aerogel-synthesized ZnO-ZrO_2.[60] After flowing CO_2, surface HCO_3^-* and CO_3^{2-}* species were observed at 1610, 1510, 1337, and 1318 cm^{-1}. The further replacement of the CO_2 flow with H_2 was followed by a rapid formation of HCOO* species (1585 and 1353 cm^{-1}) and consumption of the

https://doi.org/10.1021/acs.energyfuels.4c03013
Energy Fuels 2024, 38, 18265−18291

(bi)carbonate species. These findings suggest the instability of the carbonate species in the presence of H_2 and support the attribution of the peak at 1357 cm^{-1} to HCOO* and not to the CO_3^{2-}* species. Similar results were also observed when following the CO_2 adsorption and conversion over ZnZrOx at 315 °C in DRIFTS.[72] The peaks assigned to surface carbonate (CO_3^{2-}) and bicarbonate (HCO_3^-) species were observed during the CO_2 adsorption step at 1610, 1500, 1368, 1337, and 1074 cm^{-1}. When switching to H_2 flow, the carbonate peaks decrease with a simultaneous increase of the peaks assigned to surface HCOO* species at 2970, 2872, 2738, 1590, 1382, and 1370 cm^{-1}. After a prolonged time under a H_2 flow, peaks for surface CH_2O* species were reported at 1145 cm^{-1}. In a further stage, CH_3O* (2820 and 1059 cm^{-1}) species emerged from the consumption of HCOO* and CH_2O*.[72]

Table S1 gathers the different vibrational frequencies obtained from IR studies on a selection of metal oxides reported in this review. As shown, different peak positions were reported for the same vibrational mode, with no clear explanation of the origin of the shift. The complexity of the IR spectra can lead, in some instances, to confusion of the assignments of the peaks. In addition, little care was given in the reports to compare the stability (interaction energy) of the intermediate surface species with the catalyst, which can possibly be explained by the IR red or blue shift and further linked to the catalytic outcome. It is noteworthy to mention that the direct comparison of the peaks between the reports needs to account for the temperature at which the IR spectra were measured, since this can directly affect the intensity and position of the IR peaks. In fact, we believe that a standard protocol must be established in order to deliver a better comparison of the properties of the CTM catalysts during the reaction. The protocol can be similar to that reported by Tan et al. over Fe−Zn−Zr catalyst. As reported in Figure 4, the authors followed with in situ DRIFTS the CO_2 adsorption and CO_2 hydrogenation on the surface of the FeZnZr catalyst before and after treatment with TPABr (FeZnZr-T-*x*h) in order to study the effect of the formation and strength of interaction of the HCOO* and CH_3O* species on the synthesis of the methanol.[44] Different treatment periods were studied, from 6 h (FeZnZr-T-6h) to 72 h (FeZnZr-T-72h). However, the focus here is given to the comparison of the treated samples (as a bulk) with the untreated one. During the adsorption of CO_2, peaks attributed to surface HCO_3* (1611−1605 cm^{-1}), bidentate HCOO* (2886−2881, 2979, and 1584 cm^{-1}), and monodentate carbonate (1521, 1508, 1358, and 1340 cm^{-1}) species were reported (Figure 4a,b). When adding H_2 to the CO_2 flow, the intensity of the peaks relative to HCOO* increased alongside the reduction of the peaks from HCO_3* and carbonate species. Meanwhile, CH_3O* peaks start to emerge at around 2932, 2824, 1144, and 1054−1046 cm^{-1} (for both the treated and nontreated FeZnZr oxides) (Figure 4c,d). To better differentiate between the surface properties of the measured FeZnZr oxides, the authors followed the strength of the interaction between the intermediates and the surface, which is believed to be a key parameter in determining the reaction pathway. To study the strength of the HCOO* interaction, the evolution of the peaks corresponding to the HCOO* species was followed under thermal desorption conditions (under an Ar flow). Here, a minor decrease in the peak's intensity was noticed on the FeZnZr-T oxides in comparison to a sharp decrease over the FeZnZr oxide (Figure 4e,f). Alongside, a peak at 2226 cm^{-1}, attributed to surface CO* species (Figure 4e), was observed on FeZnZr, which was linked to the dissociation of the desorbed HCOO* species. It was thus proposed that a weaker interaction of HCOO* can cause its desorption and dissociation to CO, while only a relatively strong interaction will allow its hydrogenation to CH_3O*. The ease of desorption of the formed CH_3O* species is an important parameter to consider. When following the evolution of CH_3O* species over the different oxides, a strong CH_3O* interaction was noticed over FeZnZr oxide in comparison to the treated FeZnZr-T ones (2819 cm^{-1}), which makes the CH_3O* elimination the rate-determining step on FeZnZr and induces its lower MeOH selectivity.[44]

Having discussed the CTM reaction from a catalytic and mechanistic view, we will now shift our focus to the tandem system when combining CTM with the methanol to gasoline (MTG) reaction. It should be underlined that the system changes drastically in the tandem process. In the mechanistic part, the hydrogen that is being produced from the zeolite (essential for MTG), as well as the desorption of CH_3O* species, is the main contributor to altering the mechanism. The MTG section will be discussed further with a focus on the studied materials, the reaction mechanism, and the reaction kinetics.

3. CO_2 TO METHANOL TO HYDROCARBONS

Hydrocarbons are an important source for satisfying energy needs and chemical industry demands and are usually characterized by their carbon number and properties. DME consists of two carbon atoms but no C−C bonds and is considered an important fuel and building block. The fuel aspect is due to its lack of production of dangerous byproducts such as nitrogen oxides (NO_x) upon combustion, and its role as an intermediate in the production of valuable chemicals is well-known.[73] For these reasons the possibility of producing DME from CO_2 hydrogenation has been widely studied.[74] Liquefied petroleum gas (LPG) consists of hydrocarbons with three and four carbon atoms, i.e., mainly propane and butanes and second propylene and other light hydrocarbons,[75] in concentrations that may vary from pure C_3 to pure C_4.[75] When increasing the number of atoms, a different product is obtained, namely, gasoline, which consists of hydrocarbons with a carbon number range of C_4−C_{12} (but mainly C_5−C_{10} sometimes split into light (C_5−C_6) and heavy (C_6−C_{12}) naphtha) and octane boosters.[76] Both products LPG and gasoline are conventionally produced in refineries by several processes and often defined based on boiling point ranges.[76] However, due to the differences between the refineries, the region of operation, and the sales market, as well as the season (summer and winter gasoline composition), the exact composition of gasoline varies. In detail, gasoline mainly consists of paraffins, of which the largest part are isoalkanes, followed by alkanes and cycloalkanes. The second major fraction are the aromatics next to a small percentage of olefins as shown in Table 2. Specific components of interest are benzene and durene, the latter needing to be avoided due to its

Table 2. Composition of Gasoline

Compd	Vol (%)
Olefins	9−25
Aromatics	25−40
Total paraffins	30−90

https://doi.org/10.1021/acs.energyfuels.4c03013
Energy Fuels 2024, 38, 18265−18291

relatively high melting point. To the final blend, more compounds are added to boost the octane number and enhance the properties of the gasoline.[77−81]

The scope of this review is to study the direct production of these later two types of products (LPG and gasoline), mainly in the saturated form, with an emphasis on gasoline range hydrocarbons, from carbon dioxide and hydrogen via intermediate methanol formation. As aromatics are also important and are considered gasoline products, they are included in this review. The reason is that aromatics can be an important percentage of the final product (especially benzene, toluene, etc.) and a lot of groups are focusing on their production (without always determining all of the aromatic products that were produced). The attention is put on the effect of the reaction parameters such as temperature, pressure, GHSV, proximity of the catalysts, and of course the choice of the catalytic materials that have higher selectivity to gasoline range products. In addition, the mechanism of such catalytic systems is described. Finally, a short review of the kinetic models developed for such systems is presented.

3.1. Methanol to Gasoline. The first innovative process that allowed the production of fuels from C1 compounds (such as CO) was the Fischer−Tropsch synthesis (FTS) process, and about 50 years later, a new process was introduced, namely, methanol to gasoline.[82] MTG is a process developed by Mobil in the late 1970s and was commercialized in New Zealand with the first plant in 1985.[83] Some years later (early 1980s), a similar reaction, methanol to olefins (MTO), was introduced by Union Carbide.[82] The MTG process has many advantages compared with the FTS reaction such as the significantly higher yield toward gasoline-range products.[82] The main reasons this reaction is of such high importance are as follows: First, the hydrocarbons produced are of a relatively small range (no chains longer than C11) and very little methane is produced.[82] Second, the conversion and selectivity are high, leading consequently to high yields of isoparaffins and aromatics that increase the octane number and thus the quality of the gasoline.[82] A simplified MTO/MTG reaction (not stoichiometric) progression is shown in Figure 5.[83]

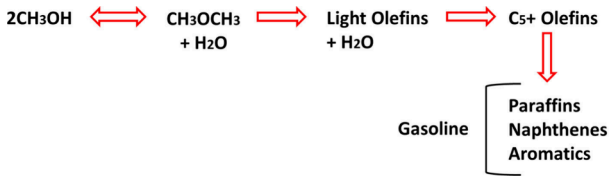

Figure 5. MTG reaction pathway with intermediate MTO.

Except for MTG and MTO, methanol can be converted to a target range of aromatics (MTAs) and in particular BTX (benzene, toluene, and xylene) following a similar way with some crucial mechanistic differences.[84,85] MTG processes are catalyzed by zeolite catalysts (aluminosilicate materials) that can offer a good gasoline (e.g., octane number). An outstanding material is ZSM-5 zeolite developed for a commercialization of the process.[83,86] Normally, the optimized conditions of the reaction are a quite high temperature of 400 °C and 15−25 bar of pressure, leading to a selectivity of 80% in gasoline-range products and LPG as the rest.[86] Although this process was a breakthrough, the fast deactivation of the zeolite ZSM-5 increased the need for further research, not only on the coking mechanism but also on different types of zeolites.[87] It was found that changing the structure of the zeolites, the aluminum content, or even adding other elements inside the structure would allow different and in some cases better performances.[86] More specifically, zeolites differing in topology have been screened throughout the years, elucidating important information such as the role of shape selectivity and pore-size gasoline cut relations. Some of the most researched topologies for the conversion of methanol to hydrocarbons are MFI (ZSM-5), CHA (SAPO-34), and TON (ZSM-22) with MFI leading the path of MTG and CHA often used for MTO.[88] Another important factor for this reaction is the production and presence of water. It has been studied and found that cofeeding water with methanol can counter the deactivation of the zeolite, but at the same time it has a negative effect on the product selectivity, boosting the selectivity toward light olefins and suppressing the aromatic production.[89] The reason for this behavior is that the strong acid sites of the zeolites are being claimed by both water and coke precursor compounds while, at the same time, these are the sites where dimerization toward paraffins or aromatics is expected to take place.[89] Despite the addition of water to improve the lifetime of MTG and MTO, more strategies have been studied such as the partial pressure of the MeOH in the feed (addition of dilutants with MeOH at the feed).[90] Another important discovery was done by cofeeding H_2 which facilitates the hydrogen transfer under high pressure, suppressing the propagation rate of the aromatics during the MTO while also keeping stable the selectivity of olefins.[90] This is, of course, relevant when coupling of CO_2 to MeOH with MTO or MTG.

3.2. Catalytic Materials for Methanol-Mediated CO_2 Conversion to Gasoline. For combining CTM and MTG, bifunctional catalysts or two catalysts in tandem, consisting of an oxide and zeolite parts, are needed. More specifically, in order to ensure the MeOH route, the oxide must be selective to MeOH when tested alone (in a reasonable temperature window). Relatively little research has been done on this direct CO_2-to-gasoline route. Most of the groups are focusing their research activities on modifying the oxide part, which consists in many cases of Zn and Zr oxides, or on coupling the oxides with small-pore zeolites toward olefins.[63,91] This is due to the high selectivity to MeOH that this material offers, as can be seen in Table 1. Moving on to the second part of the tandem process, the most used zeolite in literature is ZSM-5 (MFI topology), which is known for its ability to produce longer hydrocarbons thanks to its specific porous nature (2D + a zigzag channel) that creates the cavities needed for the hydrocarbon pool production, often one of the critical steps in hydrocarbons formation.[86,92] In Table 3, all of the examples coupling ZnZrOx with ZSM-5 for the production of longer chain hydrocarbons are presented. Li et al. tested ZnZrOx prepared by solid solution method using ZSM-5 zeolites with different Si/Al ratios (and different GHSVs), proving that higher Si/Al ratios can benefit the reaction by increasing the CO_2 conversion and decreasing the CO selectivity even though the selectivity to aromatics reaches a maximum at Si/Al = 100 (entry no. 1−5 in Table 3).[63] The same work also showed that the production of H_2O together with the presence of CO_2 in ZSM-5 leads to better catalyst stability (about 100 h without significant deactivation) by affecting the intermediate products (less polycyclic aromatics which are precursors to coke formation).[63] Moreover, a similar study was conducted by Zhang et al. (entry no. 6−13 in Table 3) and showed that increasing the Si/Al ratio indeed benefits the production of

https://doi.org/10.1021/acs.energyfuels.4c03013
Energy Fuels 2024, 38, 18265−18291

Table 3. ZnZrOx and ZSM-5 Catalysts for the Hydrogenation of CO_2 to Hydrocarbons (MeOH Route; See References 60, 63, 72, 93, and 94)[a]

No	ZnZrOx synthesis Zn:Zr (molar)	ZSM-5	Si/T(1)	Oxide/ Zeolite	H_2:CO_2, T(°C), P(bar)	GHSV ($ml/g_{cat}/h$)	CO_2 conv. %	Main product, select. %	CO select. %	ref
1	Solid solution 0.13:1	-	-	1/0	3, 320, 40	2400	n.m(2)	Methanol, 65%(3)	n.m	63
2		HZSM-5 custom purchase	25	1/1		1200	15	C2-C4, 26	48	
3			65				12	Aromatics, 17.1	43	
4			100				13	Aromatics, 41.76	42	
5			150				12	Aromatics, 39.6	34	
6	Incipient wetness impregnation 0.89:1	-	-	1/0	3, 340, 30	14400	7	Oxygenates, 52	48	93
7		HZSM5 synthesized	50	1/2		4800	10	C1-C3, 10.1	57	
8			100				8	Aromatics, 20.5	43	
9			300				6	Aromatics, 31.9	42	
10			400				6.5	Aromatics, 39	36	
11			600				6	Aromatics, 42.9	34	
12			800				6	Aromatics, 37.5	33	
13		Alkaline treatment	AT				5	Aromatics, 25.4	46	
14	Co-precipitation 1:6	-	-	1/0	3, 320, 40	21818	3.5	Methanol, 68	31	94
15		H[Al]ZSM-5	80	1/2		7200	10	Paraffins, 35	38	
16		H[Ga]ZSM-5	80				7	Paraffins, 25	36	
17		H[Fe]ZSM-5	80				8	Aromatics, 47	33	
18		H[B]ZSM-5	80				6.5	Oxygenates, 42	58	
19		H[Al]ZSM-5	300				5	Aromatics, 42	32	
20		H[Ga]ZSM-5	300				9	Aromatics, 46	33	
21		H[Fe]ZSM-5	300				6	Aromatics, 37	32	
22	Aerogel, 1:4	-	-	1/0	3, 340, 40	21200	8.6	Oxygenates, 50.2	49.8	60
23	Aerogel, 1:20	HZSM-5 custom purchase (4)	68	1/2		7200	15	Aromatics, 33.6	58.4	
24	Aerogel, 1:8						16	Aromatics, 49.9	34.3	
25	Aerogel ,1:4						15	Aromatics, 37.7	46.8	
26	Aerogel, 1:1						11	Aromatics, 18.2	73.1	
27	Co-precipitation 1:6.7	-	-	1/0	3,315,30	n.m.	11.1	Oxygenates, 57.7	41.5	72
28		HZSM-5 0.73(5)	48	1/1		1020	17.5	Aromatics, 45.9	23.8	
29		HZSM-5 0.73T(6)	43				14.1	Aromatics, 41.8	38.4	

[a]The − in the ZSM-5 column means no zeolite is used and the result is a bare CO_2-to-methanol experiment for comparison. Notes: (1) nominal; (2) n.m = not mentioned; (3) not specified if it is hydrocarbon selectivity or product selectivity; (4) post-treated to create mesoporosity; (5) the chain-like HZSM-5 crystals should grow along with the orientation of *b*-axis length 0.73 μm of the nanocrystal of the zeolite; (6) hydrothermally treated.

Table 4. Catalysts in Tandem for CO_2 Hydrogenation to Hydrocarbons (Methanol Route; See References 44, 65, 68−70, and 95−98)[a]

No	Oxide	Zeolite	Preparation	H:CO_2 /T(°C) /P(bar)	GHSV ($ml/g_{cat}/h$)	CO_2 conversion %	Main product, selectivity %	CO selectivity %	ref
1	CuZnAlOx	HZSM-5	Physically mixed	3, 340, 30	9000	30	C5+, 2.75	95	65
2	ZnAlOx	-		3, 320, 30	12000	5.2	Methanol, 25.2	55	69
3		HZSM-5	Mixed with grinding	3, 320, 30	6000	5.2	Aromatics, 29.6	42	
4	FeZnZr	-	-	3, 340, 50	4500	19	Oxygenates, 20	80	95
5		HY	Physically mixed	3, 340, 50	3000	18.5	i-C4, 19.4	55	
6		-		3, 340, 50	3750	13.9	Oxygenates, 37.7	34.8	44
7		HZSM5	Core-shell(1)	3, 340, 50	3750	18.8	i-C5+, 37.9	29.3	
8		-		3, 340, 50	3000	16	Oxygenates, 7.8	89.6	96
9		HY	Core-shell	3, 340, 50	3000	15.6	i-C4, 22.7	41.8	
10	ZnCrOx	-		3, 350, 50	2000	38.3	Oxygenates, 45.1	54.1	70
11		ZnZSM-5	Mixed with grinding	3, 350, 50	2000	30.5	C6+, 16.5	60.8	
12		HZSM-5	Not mentioned	3, 340, 30	9000	8.1	C5+, 24.11	60.6	65
13	Cr_2O_3	-		3, 350, 30	2400	11.2	Methanol, 68.84	29.1	68
14		HZSM-5	Physically mixed	3, 350, 30	1200	33.6	Aromatics, 41.45	41.2	
15		-		2.6, 350, 30	n.m.(2)	11	Oxygenates, 46.3	52.5	97
16		HZSM-5@SiO2	Mixed with grinding	2.6, 350, 30	1200	22.1	Aromatics, 45.5	35.1	
17	In_2O_3	-		3, 340, 30	9000	15	Methanol, 22	72	65
18		ZSM-5	Physically mixed	3, 340, 30	9000	14	C5+, 44	45	
19	InCo	-		4, 300, 50	15000	17	Methanol, 64	30	98
20		ZnBEA	Dual layers	4, 300, 50	8100	17	iC4-C7, 54	35	

[a](1) FeZnZr-T-24h, the oxide prepared by treatment with TPABr; (2) n.m= not mentioned.

aromatics, reaching a maximum at Si/Al = 600. It needs to be underlined that it is not easy to compare the two studies, and one should be very cautious when doing so, because of the different oxide/zeolite ratios, which play a major role in this

https://doi.org/10.1021/acs.energyfuels.4c03013
Energy Fuels 2024, 38, 18265−18291

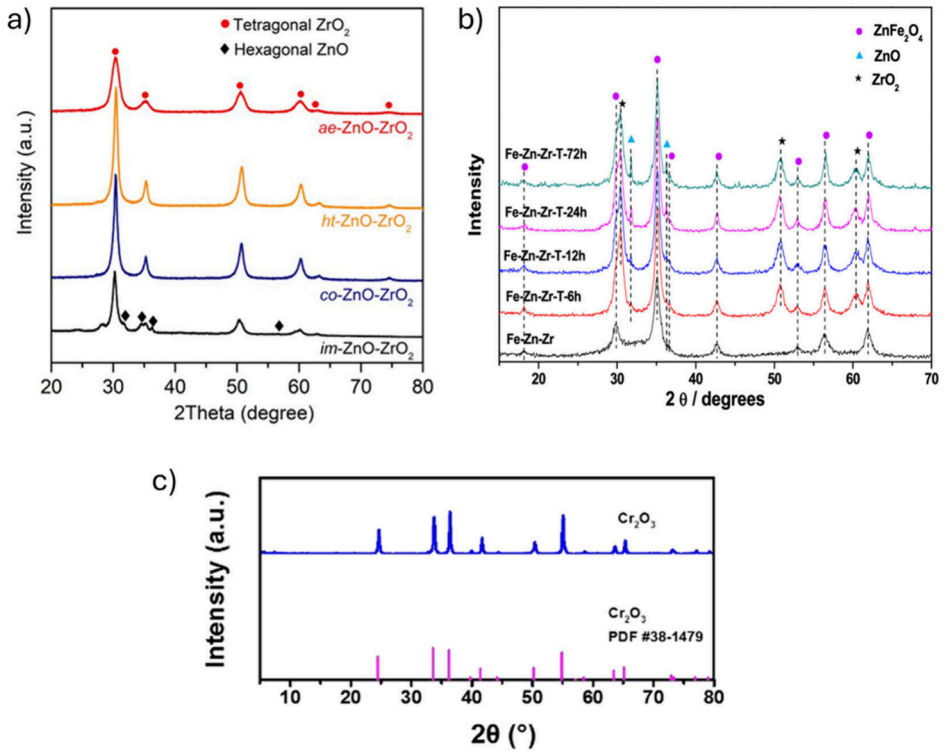

Figure 6. XRD patterns of (a) ZnZrOx prepared with different methods (ae, aerogel; ht, hydrothermal; co, coprecipitation; im, impregnation). Reproduced with permission from ref 60. Copyright 2020 American Chemical Society. (b) Pure FeZnZr and treated FeZnZr with TPABr over different hours (FeZnZr-T). Reproduced with permission from ref 44. Copyright 2021 American Chemical Society. (c) Cr_2O_3. Reproduced with permission from ref 97. Copyright 2019 John Wiley and Sons.

reaction, in addition to the differences in the reaction conditions. Recently, Shah et al. (entry no. 14−21 in Table 3) altered the acidic properties of HZSM-5 by substituting the heteroatoms of the zeolitic framework concluding that H[Fe]ZSM-5 with Si/T = 80 showed 47% selectivity to aromatics at an 8% CO_2 conversion. In addition, Zhou et al. synthesized ZnZrOx with different methods, concluding that aerogel as synthesis method (sol−gel combined with supercritical drying) leads to very active material due to the high number of oxygen vacancies (measured by electron paramagnetic resonance (EPR)) that is present, enhancing the CO_2 conversion as discussed earlier in the mechanistic part (entry no. 22−26 in Table 3).[60] Wang et al. studied the correlation between the *b*-axis length of the ZSM-5 chain-like nanocrystals and the selectivity of the products, hypothesizing that when the length increases, *p*-xylene selectivity also increases, whereas when the length decreases, the selectivity toward tetramethylbenzene increases.[72] As seen in entry 28 of Table 3, the samples with *b*-axis length at 0.73 μm were found to have a conversion of 17.1% with a very low CO selectivity (23.8%).

Except for ZnZrOx, a few other metal oxides have been tested in combination with ZSM-5 zeolite as presented in Table 4. It is noticeable, based on Tables 2 and 3, that most research reports have been conducted on Zn-containing materials. Starting from the most conventional catalyst for converting syngas to MeOH (CuZnAlOx), which, once tested in the CO_2 conversion to gasoline, does not appear to be a good choice. Indeed, even though CuZnAlOx presents the highest CO_2 conversion, this catalyst was extremely selective toward CO (entry no. 1 in Table 4).[65] At the same time, when Cu is not added to the oxide, the catalyst performs better, reaching a selectivity of 30% toward aromatics, but at a much lower CO_2 conversion (entry no. 3 in Table 4).[69] The same group studied the effect of adding CO in the feed gases since the rWGS reaction is at equilibrium, meaning that the effect can only be positive by suppressing the unwanted reaction. One of the first groups that studied the production of isoalkanes from CO_2, the Tsubaki group, studied the combination of Fe−Zn−Zr oxide with an HY zeolite (FAU topology) proving for the first time the possibility of such a reaction path that results in a high selectivity to isobutane (entry no. 5 in Table 4).[95] Wang et al. further introduced a core−shell method for preparing the bifunctional catalyst, with the Fe−Zn−Zr oxide being the core and the zeolite being the shell. This was done by adding aqueous diluted silica on the metal oxide part and then mixing that with the zeolite.[96] What was found (in two research works from the same group) is that this method can actually increase the production of the targeted fuels when HZSM-5 (or a combination of two zeolites) is used as the shell (entry no. 6−9 in Table 4).[96] Another important element in this list is Cr, either as pure Cr_2O_3 or in combination with Zn (entry no. 10−16). It can be mentioned that when only Cr oxide is used, the selectivity of aromatics can reach 45.5% at 22% conversion when the core−shell technology is applied on HZSM-5 using a shell of amorphous SiO_2 on the latter.[97] Gao et al. used the coprecipitation method to prepare different oxides in combination with HZSM-5. Among them, In_2O_3 exhibited the best performance with the highest CO_2 conversion and C5+ selectivity among hydrocarbons (entry no. 18 in Table 4).[65] The ratio of oxide/zeolite and the proximity were also studied in the same work, while some tests were also performed on a lab-pilot scale (scaled up fixed bed reactor with additional steps such as recycling to simulate the

https://doi.org/10.1021/acs.energyfuels.4c03013
Energy Fuels 2024, 38, 18265−18291

industrial conditions) and industrially more relevant conditions (15 g_{cat}).[65] Dokania et al. introduced a new material, InCo, to study the reaction together with acidic HBEA zeolite and ZnBEA, resulting in high selectivity to isoparaffins among hydrocarbons and increased lifetime of the zeolite when Zn is added by incipient wetness impregnation (entry no. 20 in Table 4).[98]

An interesting observation is that some of these oxides (FeZnZr, ZnAlOx, and In_2O_3) when tested pure, at the same conditions and the adequate GHSV, produce CO as a main product with higher selectivity than that of MeOH (or oxygenates), and at the same time when coupled with the zeolite, their selectivity to CO drops. On the other hand, for the materials that give oxygenates when tested pure (ZnZrOx, Cr_2O_3, and InCo), there was a slight increase in CO selectivity when the zeolite was added physically. This is a clear indication that it is difficult to distinguish which is the main intermediate and which reaction pathway is followed each time, and researchers should be very careful when claiming a specific reaction path. Lastly, the importance of testing the oxide pure as a reference for comparison must be highlighted, and research works that do not present these data make the understanding more difficult.

3.3. Characterization of the Catalytic Materials. Having listed the major materials reported in the literature for the production of gasoline-range hydrocarbons from CO_2 through MeOH, a closer look at some key characterization details of those materials will be discussed now. To start, FeZnZr oxides show an XRD pattern indicating the presence of mainly the spinel phase $ZnFe_2O_4$ when, at the same time, the dispersion of ZnO and ZrO_2 is so high that no peaks were observed (Figure 6 b).[44] This was also proven by TEM (transmission electron microscopy) images, where crystals of both ZnO and ZrO_2 were detected on the surface of the $ZnFe_2O_4$ phase.[44] In addition, when the group added a hydrothermal treatment step, the peaks of the XRD pattern were more intense, indicating a stronger interaction between Fe and Zn.[44] The more the time of the treatment was increased, the larger the ZnO crystal size was, leading to the appearance of reflections in the XRD. Tetragonal ZrO_2 appeared but remained stable independent of the treatment time.[44] When the oxide is coupled with the zeolite (core−shell structure), a typical XRD pattern for the zeolite was observed while SEM images proved the positioning of the zeolite as the shell, leading to the conclusion that the shell process did not harm the primary crystal structure of both catalysts.[96]

Moving to In_2O_3 materials, when treated with a mixture of H_2/CO at 340 °C for 8 h, the XRD pattern revealed the complete reduction of the oxide into metallic In.[65] In addition, when exposed to reaction conditions (H_2 and CO_2 mixture), at the same temperature, the crystal size of the oxide kept increasing during the first 4 h and then remained at a stable size.[65,99] On the other hand, the InCo (not supported) catalyst shows the XRD patterns attributable to Co_3O_4 and $In(OH)_3$ before the reaction and reflections of metallic Co, In_2O_3, and $Co_3InC_{0.75}$ after the reaction.[100] This highlights the beneficial role of Co in avoiding the formation of a metallic In phase. Having confirmed these findings by STEM (scanning transmission electron microscopy) and further characterization, the group came to the conclusion that the active phase, capable of converting CO_2 selectively to MeOH, is the oxidized In−Co layer, which exists around metallic Co.[100] As for the coupling of InCo with BEA and ZnBEA zeolites, the XRD patterns of the zeolites indicated a typical mix of polymorphs, while HAADF-STEM imaging showed a homogeneous distribution of the extraframework Zn cations onto BEA zeolite.[98]

The research groups using ZnZrOx all demonstrated XRD patterns (Figure 6a) that indicate the presence of tetragonal ZrO_2 with well-dispersed Zn species.[60,63,72] It has also been confirmed that, even after reduction with H_2 at 350 °C, no new peaks were formed, yet the existing ones slightly increase.[72] The only major difference was observed for the material prepared with the aerogel procedure where XRD revealed the presence of hexagonal ZnO, and at the same time, TEM showed a three-dimensional structure with a high surface but a smaller particles size.[60] TEM imaging also proved that the further addition of Zn leads to larger particles and the nanoparticles formed linked chains.[60] When the zeolites were added by physical mixing or grinding, a good dispersion of the oxide on the zeolite was revealed with XRD patterns and SEM images, which potentially highlights a physical closeness of the two components while maintaining their structures.[63,72] All zeolites exhibit no impurities and great crystallinity,[63] but the work of Wang et al., who studied the role of the *b*-axis length of the ZSM-5 zeolite, showed SEM and TEM images that proved that the addition of *n*-octyltrimethoxysilane in the zeolite synthesis leads to chain-like morphology.[72]

The XRD patterns of ZnAl oxides show the cubic $ZnAl_2O_4$ gahnite as a main phase with low-intensity peaks of ZnO. In combination with SEM and TEM images, it was shown that the oxide is porous and consists of very small nanoparticles.[69] Moreover, the spaces in the lattice show the spinel structure of the oxide.[69] The ZnCr oxides reveal a spinel crystalline structure which is nonstoichiometric.[70] SEM and TEM images indicate the good contact between the oxide and zeolite materials after grinding them together, which was concluded by the uniform appearance of the particles.[70] Finally, the last material examined, Cr_2O_3, showed a resemblance with eskolaite which has a hexagonal structure as seen on the XRD and an excellent stability with unchanged crystal size (SEM images) and XRD pattern even after 100 h on stream.[68] Figure 6 shows the XRD patterns of some of the materials discussed.

Another important part of the characterization of the oxide materials is the specific surface area, e.g., given by the Brunauer−Emmett−Teller (BET) method after N_2 physisorption. Oxides need to activate CO_2 on their surface, often on oxygen vacancies where CO_2 can coordinate. In Table 5, the areas of some of the oxides are presented. What can be seen is that among all of the materials, only for a particular ZnZrOx a high specific surface area of around 300 m^2/g was documented (in catalysis for CO_2-to-gasoline context) while all the other oxides range between 20 and 160 m^2/g. The values obtained from different methods of making ZnZrOx also differ greatly (Table 5). The oxygen vacancies can be formed both on the surface and in the bulk phase of the material, yet the ones on the surface are more favorable (kinetically and thermodynamically).[60] Zhou et al. investigated in detail ZnZrOx materials synthesized with different methods, reaching the conclusion that more oxygen vacancies (measured using EPR) mean a higher methanol (or DME) rate of formation.[60] The authors found that the decrease in the surface areas due to the difference in the synthesis methods leads to a decrease in the density of oxygen vacancies: ae-ZnZrOx > ht-ZnZrOx > co-ZnZrOx > im-ZnZrOx.[60]

https://doi.org/10.1021/acs.energyfuels.4c03013
Energy Fuels 2024, 38, 18265−18291

Table 5. BET Surface Area Obtained from N_2-Physisorption for the Different Oxides

Catalyst	BET (m^2/g)	Ref
FeZnZr	76	44
FeZnZr-T-6h→72h	41→28	44
FeZnZr	94	96
In_2O_3	121	65
InCo	30	98
ZnAlOx	151	69
Cr_2O_3	12.9	68
ZnZrOx	319	72
ae-ZnZrOx[a]	124	60
co-ZnZrOx[a]	53	60
im-ZnZrOx[a]	23	60

[a]ZnZrOx produced by ae = aerogel method, co = coprecipitation method, or im = impregnation method.

In contrast with the oxides, zeolites have a very high surface area, which is only slightly affected by the variation of the Si/Al ratios or the addition of metals or cations (e.g., Zn) instead of the framework aluminum or the proton countercation. Typically, for HZSM-5 the surface area ranges between 300 and 500 m^2/g.[65,69,95,96] In comparison, the most reported HBEA and HY zeolites show higher BET surface areas of around 550 and 525−750 m^2/g accordingly.[95,96] In the study on the *b*-axis of ZSM-5 it was observed that the longer the axis of the zeolite, the larger the surface area, ranging from 423 m^2/g for a length of 0.16 μm to 620 m^2/g at a length of 1.41 μm.[72]

3.4. Catalytic Results for CO_2 to Gasoline through Methanol. After reviewing the different materials that have been studied and their first indicative performances (Tables 3 and 4) and characterizations, we aim to critically represent and compare their catalytic activity. Figure 7 groups the reaction conditions for the reported catalytic screenings from an oxide point of view and, more importantly, the frequency at which the catalysts were tested under such conditions. This frequency is represented by the circles; the wider the circle is, the more a catalyst has been tested, i.e., under different modifications on the synthesis methods, different GHSV, different bed configurations, or combinations with different zeolites.

The frequency circles show that ZnZrOx has been tested most extensively in the artifact, followed by FeZnZr and ZnAlOx. In addition, it is noticeable that the largest diversity of catalysts is found to have been tested at 30 bar, while only ZnZrOx has been tested at 40 bar. Moreover, as can be concluded from Figure 7, most research (in the scope of this review) has been conducted in a the temperature range of 300 to 350 °C. There are materials that have not been tested at different pressures or temperatures, indicating that there are still opportunities for further optimization.

Since all groups have been testing a plethora of catalytic materials (consisting of two catalytic functions) and conditions, it is very difficult to safely compare catalytic output. Hence, we deem it essential to try to represent the different kinds of products in association with the conditions. While such plots are skewed by research choices, the Figure 8 panels indicate the frequency in which different types of products have been produced as the main product by different catalysts in different temperatures and pressures (even though conditions other than *T*, *P*, or GHSV and catalysts fluctuate). Most C5+ products are produced as the main product at tests at a temperature of 340 °C, while most of the aromatics are encountered at equal or lower temperatures (340 and 320 °C), as seen in Figure 8a. In the case of olefins (not covered here; e.g., see ref 101), higher temperatures are generally needed (>350 °C) in order to promote the different mechanisms (e.g., hydrocarbon pool chemistry).[102]

As for the pressure (Figure 8b), a trend can be noted for the aromatic products since they are mostly produced during experiments at lower pressures. As the pressure increases in different reports, C2−C4 products are more often found as the main product. For C5+ products, there is no obvious trend as they seem produced with the same frequency as experiments at 30 and 50 bar. The GHSV (Figure 8c) that is chosen by researchers varied between 500 and 12000 (mL/g_{cat})/h. C5+ products were the main products in experiments at higher

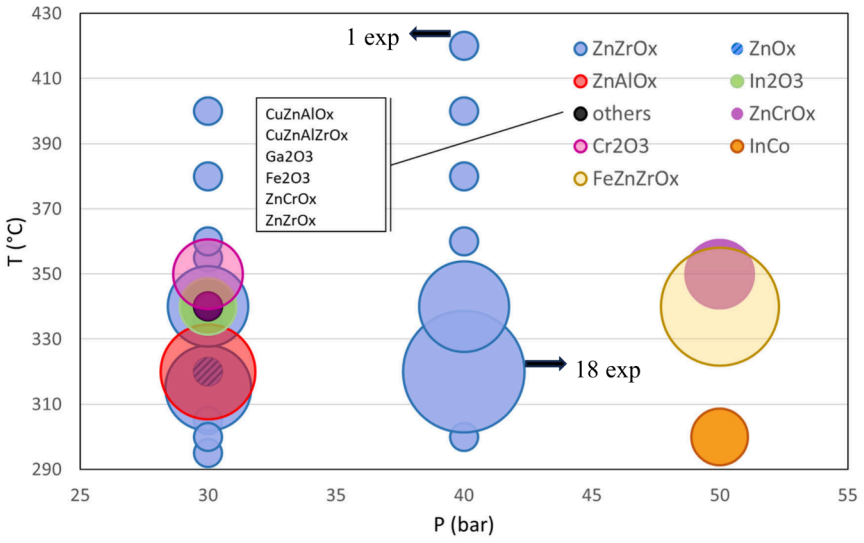

Figure 7. Frequency of conditions per oxide chosen by researchers investigating MeOH mediated CO_2 to gasoline-range products. The frequency is represented by the size of each circle with a minimum of one experiment (smallest circle) and maximum of 18 experiments (biggest circle), and the coordinates of the center of the circle illustrate the temperature and pressure. With the black circle, all experiments done, one time, at 30 bar and 340 °C, which otherwise cannot be distinguished due to the same position and size of the circles.

https://doi.org/10.1021/acs.energyfuels.4c03013
Energy Fuels 2024, 38, 18265−18291

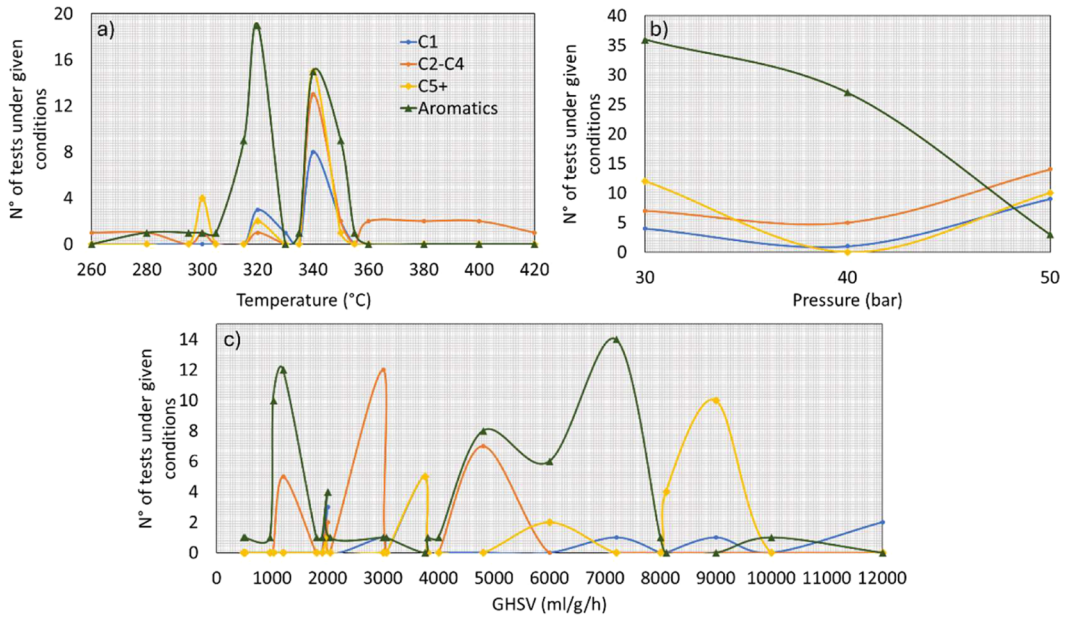

Figure 8. Representation of frequency of investigation of different catalytic systems under different (a) temperatures, (b) pressures, and (c) gas hourly space velocities (GHSVs) and their main product produced. The division of the product categories is established based on information given by researchers taking into account the often lack of specific product distribution. Each experiment is evaluated based on the main product (CO is not taken into account) meaning that each experiment is linked with its main product, and this couple is only presented as one test.

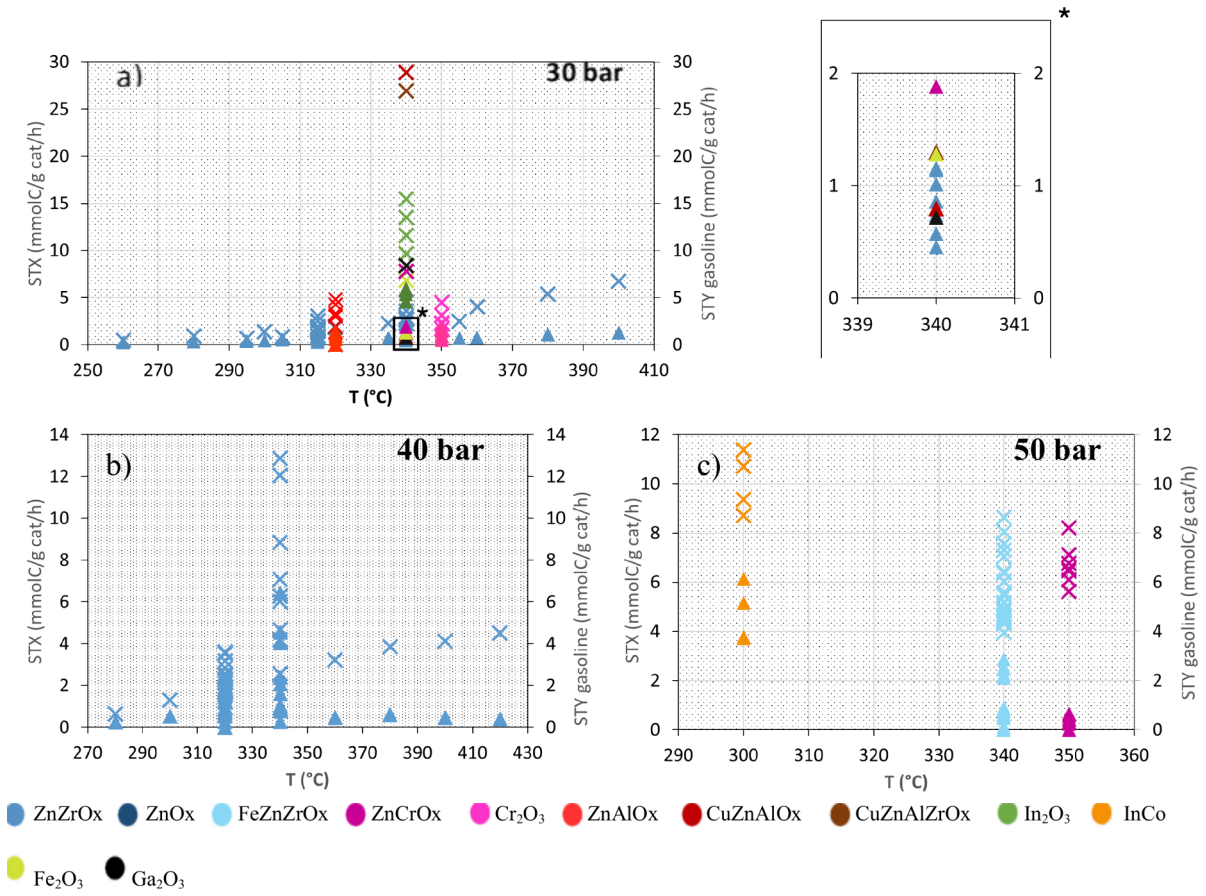

Figure 9. Effects of temperature of reaction on different catalytic systems on space time conversion of CO_2 (STX, X) and space time yield of gasoline-range products (STY, ▲) under stable pressure: (a) 30 bar (box marked with asterisk (*), zoomed-in image of the marked area), (b) 40 bar, and (c) 50 bar. The catalytic systems consist of an oxide (different colors) and a zeolite (not presented).

GHSVs (8000−9000 (mL/g_{cat})/h), while C2−C4 were the main products at lower (1000−5000 (mL/g_{cat})/h). Aromatics were the main products in reactions in both lower and relatively high GHSVs. Figure 8 is meant as an indicative

https://doi.org/10.1021/acs.energyfuels.4c03013
Energy Fuels 2024, 38, 18265−18291

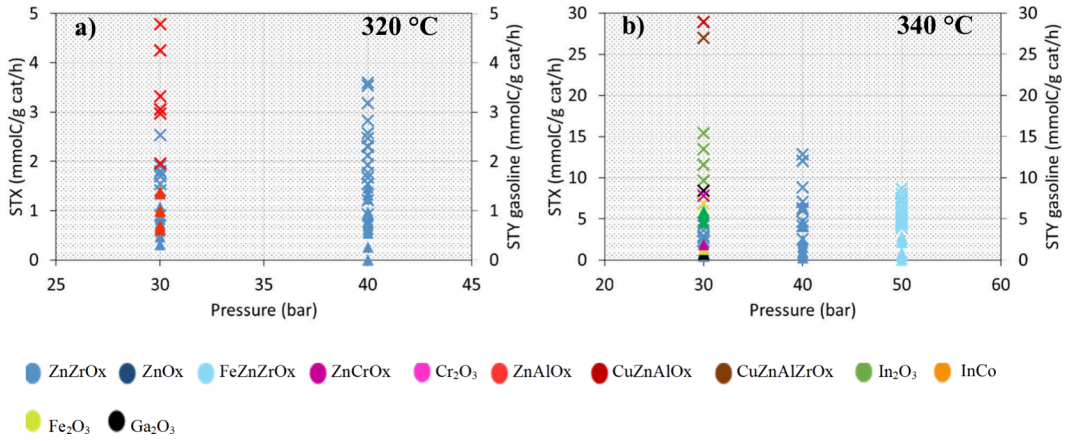

Figure 10. Effects of pressure of reaction on different catalytic systems on space time conversion of CO_2 (STX, X) and space time yield of gasoline-range products (▲) under constant temperature: (a) 320 and (b) 340 °C. Note the different scale ranges of panels a and b.

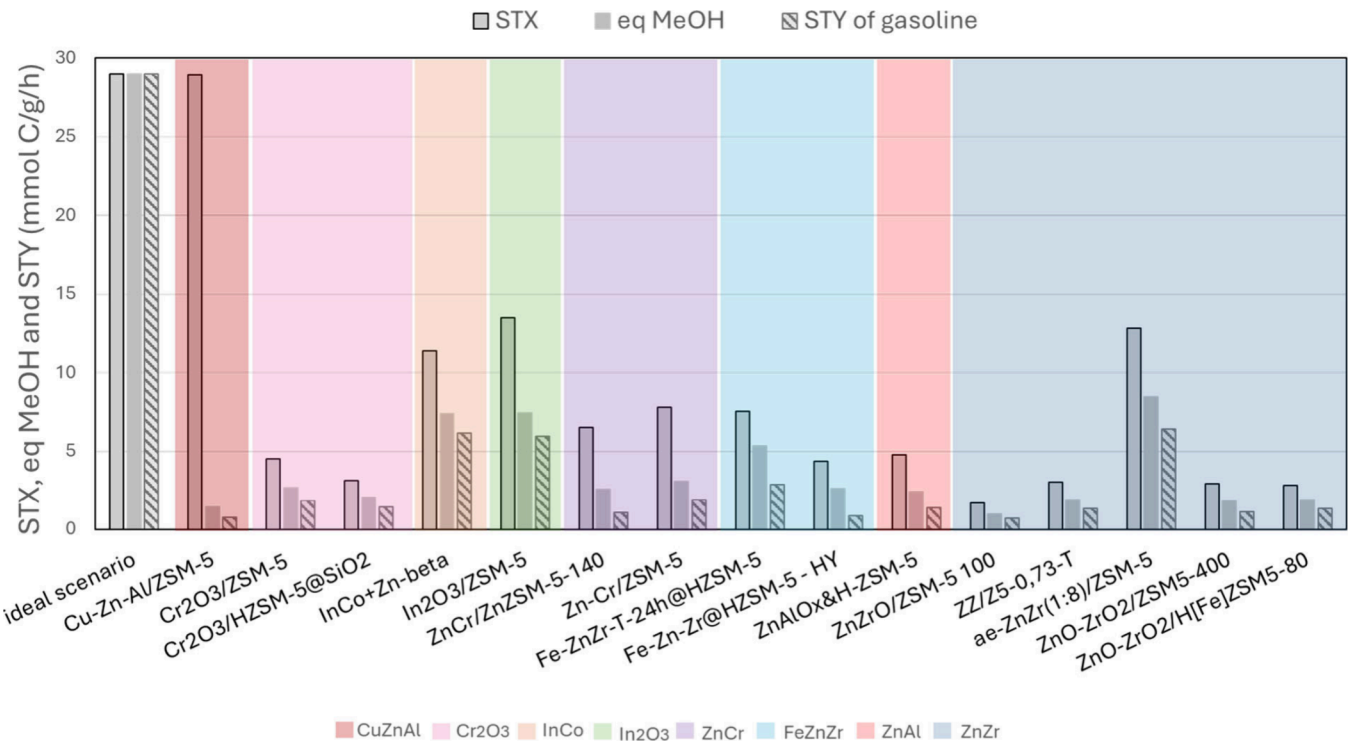

Figure 11. Catalytic systems with the highest space time yield (STY) of gasoline of each study on direct methanol-mediated conversion of CO_2 to gasoline-range products. The space time conversion of CO_2 and the equivalent of methanol (eq MeOH, assumption that all products except CO are produced through methanol as the intermediate product) are also illustrated. The names of the systems are given as mentioned by the researchers who published the works.

overview of the materials presented in the literature with a focus on their testing regime frequency but often includes (or reflects) choices made by the authors. They should not necessarily be interpreted as sound conclusions, and therefore, the effect of the conditions chosen and the products detected will be studied next in more depth.

3.4.1. Reaction Conditions for CO_2 to Gasoline through Methanol. In order to compare the effects of the conditions across different materials and studies, some variables needed to be eliminated. For this reason GHSV, CO_2 conversion, and feed gas ratios have been combined into one variable named STX—the space time conversion, given as the amount of CO_2 (mmol) that has been converted per gram of catalyst per hour—and STY—which is the space time yield of gasoline-range products (all products with carbon number > 5 containing the aromatics) as mmol of C produced per gram of catalyst per hour—where C5+ products, both alkanes and aromatics, are described as gasoline. Figure 9 investigates the effect of the temperature at a given pressure. Dividing all of the different catalysts from the literature into categories based on the pressure used, it can be noted that most tests have been conducted at a pressure of 30 bar, followed by 50 bar and finally 40 bar. The highest STX noted is at 30 bar, reaching a value of ≈30 mmol of CO_2 converted g_{cat}^{-1} h^{-1} for the physically mixed tandem CuZnAlOx/ZSM-5,[65] although very low STXs are also noted for catalysts tested at the same pressure. It must be underlined that STX in itself does not provide enough information without STY as in the case of

https://doi.org/10.1021/acs.energyfuels.4c03013
Energy Fuels 2024, 38, 18265−18291

CuZnAlOx/ZSM-5 the conversion might be very high, but since the main product is CO (Table 3), the STY to desired products is very low. All materials tested at 50 bar show an STX ranging from 4 to 12 $mmol_{CO_2\ converted}\ g_{cat}^{-1}\ h^{-1}$. What is also obvious is that most research groups that work at high pressures of 50 bar work at a temperature of 340 °C although relatively high STX and very high STY have also been observed at a temperature of 300 °C (InCo), meaning that it would be interesting to investigate the lower temperature region as well for different materials at high pressure where there seems to be a gap in the state of the art.

In the same way, Figure 10 examines the effect of the pressure at a constant temperature. The temperatures displayed (320 and 340 °C) are the ones where most data in literature were found. Some of the reports detail the effect of changing the reaction temperature. In all cases, the conversion of CO_2 is increased with increasing temperature; however, the STY of the desired products either reaches a maximum and then starts dropping or keeps increasing but at a lower rate. This is due to the increase in the CO selectivity at higher temperatures.

Although this representation is a good indication of the CO_2 (and STY) conversion dependency, it obscures the effect of CO selectivity (and thus the extent of the competing rWGS reaction). For this reason, Figure 11 presents the equivalents of MeOH for the most interesting catalysts alongside the STX and the STY of the gasoline-range products. The equivalents of MeOH parameter is calculated as the theoretical amount of MeOH that would have needed to be produced (by the oxide) assuming that all hydrocarbons are produced through methanol. In an ideal scenario, the best material for this reaction should have a high STX (e.g., close to 30 $mmol_C\ g^{-1}\ h^{-1}$), which will then result into the full conversion toward the desired products (C5+ in this case), while, at the same time, all products should derive from oxygenates as an intermediate step (eq MeOH). Comparing the right bar (STY) versus the middle bar (eq MeOH) indicates the selectivity in the MeOH-derived products (e.g., equally high when methanol converts to gasoline and not to C2−C4), while the middle bar versus the left bar indicates losses to CO. It is clear that while some materials' high STX reflects in a high STY (such as for the InCo catalyst), others show the opposite behavior (CuZnAl catalyst exhibits very high STX but very low STY of gasoline) due to extensive CO production.

This is due to the enhanced rWGS activity in these CO_2 to gasoline conditions, which are harsher than those in classic CO_2 to MeOH conditions. From Figure 11, it becomes obvious that In_2O_3/ZSM-5 has one of the best performances, very closely followed by ae-ZnZr/ZSM-5 and InCo+beta. In addition, even though the selection of the zeolite is a very important factor, only limited types of topologies have been investigated. Gascon and co-workers have shown that the change in the zeolite topology can largely impact the products selectivity, as for example, 10MR zeolites (such as ZSM-5) have optimal effects via oligomerization reactions.[103] However, zeolites with larger pores can increase the selectivity to longer, mostly saturated hydrocarbons, such as the BEA zeolite (12MR), which exhibits high performances when combined with InCo, but it has not been tried yet with many other oxides.

3.4.2. Effect of Amounts and Proximity in Tandem Systems. In the light of nomenclature, a bifunctional catalyst is one material (one catalyst structure) with two functions embedded (e.g., a Pt impregnated and still acidic H-zeolite) or a hybrid core−shell; and not a physical mixture of two catalysts. Both can be considered a tandem system in the context here. However, in CO_2-to-hydrocarbons, the borders between physically mixed catalyst pellets, consecutively stacked (but separate) catalyst beds, or bifunctional catalysts are murky, especially when considering the option of mortar mixing the powders before the pelletization.

Before going into details on the proximity of the two materials (i.e., how the two active catalytic materials are geometrically arranged with respect to each other), one needs to take into account the ratio in which they will be used. Among the studies fitting the scope of this critical review, only two have explored different oxide to zeolite ratios, and these are seen in Figure 12. The first group tested two different ratios

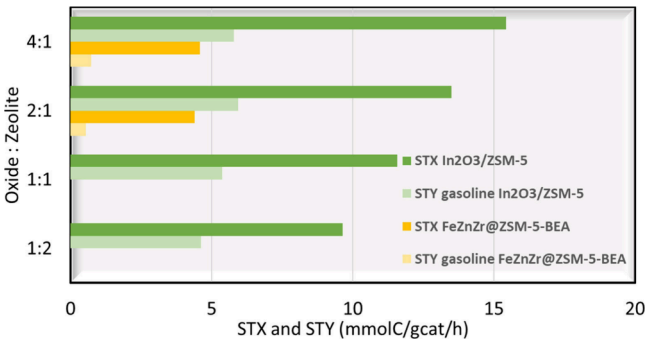

Figure 12. Effect of the oxide to zeolite weight based ratio. The space time yield (STY) of gasoline and the space time conversion of CO_2 (STX) are illustrated. The names of the systems are given as mentioned by the researchers who published the works.

for the core−shell FeZnZr oxide and zeolite (4:1 and 2:1 of oxide:zeolite).[96] It was noticed that by increasing the amount of the oxide, a slight increase in both STX and STY of gasoline products was observed. However, only limited information can be extracted since the ratio was nominal and could be altered during the synthesis stage and was not studied for multiple values. A more in-depth investigation was reported by trying several oxide:zeolite ratios using In_2O_3 and HZSM-5 (assuming a physical mixture of the materials since it was not clearly stated).[65] As expected, the increase in the amount of oxide will lead to higher STX, since CO_2 conversion primarily takes place on the oxide. On the other hand, it seems that, at an optimum ratio of 2:1, the STY of gasoline products reaches a maximum. A further increase in the oxide amount does not affect it positively. It should be mentioned that the configuration of the catalytic bed plays a role in the significance of the ratio of the oxide and zeolite. However, this has not been studied, which does not allow extracting conclusions.

As mentioned before, the proximity between the two catalytic functions likely plays an important role in the process.[104] Some research reports have conducted studies on the catalytic bed configuration in light of understanding the proximity effect on the catalytic outcome. Most frequently, a mixed bed is used, where the oxide and the zeolite are mixed together before loading them into the reactor. This mixing can be done for the pelletized samples ("physically mixing the two types of pellets") or for the powder samples ("mortar mixing" followed by grinding and pelletizing). Besides the mixed bed configuration, dual bed approaches are also encountered where

https://doi.org/10.1021/acs.energyfuels.4c03013
Energy Fuels 2024, 38, 18265−18291

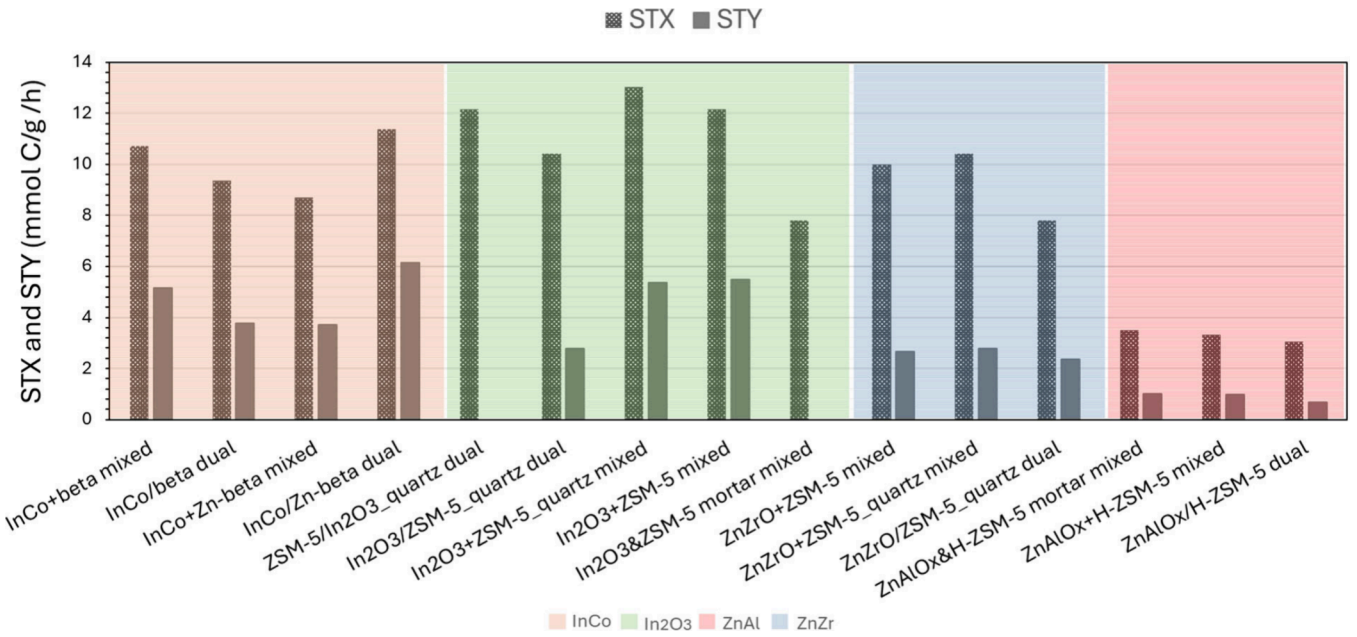

Figure 13. Effect of the proximity between the two parts of the tandem systems. The space time yield (STY) of gasoline and the space time conversion of CO_2 (STX) are illustrated. The names of the systems are given as mentioned by the researchers who published the works. Mixed = physical mixture of pellets; dual = two separate layers; mortar mixed = mixture after grinding; and quartz = dilution with inert quartz.

the two materials are placed as two separate layers with or without a thin inert layer in between (usually quartz sand). This research is currently at a very preliminary level, leaving a big gap in the understanding of how the two different reactions contribute to the final product and influence each other. Only four research works in this particular direction could be identified and are presented in Figure 13. First, when the two materials are added as separate layers, the idea is that oxygenates must be produced on the first layer and these oxygenates will be converted down flow into hydrocarbons on the second layer. Thus, when zeolite is used as the first layer, no STY of gasoline products was observed and the feed gases are directly converted on the oxide layer, giving the expected STX (experiments conducted on In_2O_3 and ZSM-5).[65] Only two of the groups have tested and compared the results from physical and mortar mixing methods.[65,69] Interestingly, while in one case (ZnAlOx and ZSM-5), no significant difference was noticed, in the second case (In_2O_3 and ZSM-5) it was indicated that the mortar mixing favored the formation of MeOH and CH_4. A possible explanation could be the presence of (mobile) In that could alter the function of the zeolitic material, but no further research has been done. In addition, when comparing the physical mixing with the dual bed configuration, the physical mixture shows a slightly better performance in almost all cases, as both the STX and the STY to desired products are higher when the catalysts are mixed. The only exception is seen for the system of InCo and ZnBEA (Figure 13) and this difference was ascribed to the possible migration of the oxide elements onto the zeolite, leading to higher Zn and InCo proximity, which can negatively affect the reaction.[98] Based on Figure 13 and its interpretation, it is clear that this aspect has not been studied enough. Even in cases where experimental data exist, not enough explanation and research has been done to prove how the proximity affects the discussed reactions.

The fact that closer proximity benefits the reaction selectivity toward targeted products has been studied using a different system, using a bioderived platform (rice husk) during synthesis of ZnZrOx/ZSM-5 @RH, where ZnZrOx is synthesized from ZnZrMOF precursor. The distance between ZnZrOx and ZSM-5 was altered by adjusting the amount of rice husk used during synthesis, showing that increasing the proximity can increase the aromatic content selectivity. However, even though the ratio between oxide and zeolite is kept stable, the total amounts are adjusted due to the different synthesis amounts, leading to slight differences in conversion levels.[105]

3.5. Mechanism of the Tandem System. Controlling the hydrocarbon distribution in CO_2 hydrogenation is a challenging task due to the complex reaction mechanisms involved inside the zeolite pores and the wide variation of the catalyst properties. The strength of the acid sites, their density, and accessibility, in addition to the steric effect induced by the different pore sizes, could affect the selectivity toward specific hydrocarbons. In general terms, ZSM-5 zeolites (MFI topology with 10MR channels) demonstrate selectivity toward the formation of aromatics, while in MOR topology (with larger 12MR channels) the olefins production is enhanced. On the other hand, FAU and BEA topologies were found to be more selective toward isoparaffins. Below, we summarize the mechanistic insights from the reported studies, highlighting the key intermediate steps and the effect of the bifunctional catalysts in the production of gasoline from CO_2 hydrogenation. We limit the discussion here to MTG insights from tandem systems, as the literature on MTG (MTH) is extensive.

As in the case of CTM (Section 2.2), the reaction mechanism in the MTG part of the tandem was mainly followed by using IR spectroscopy techniques. In the most standard protocol, the CO_2 hydrogenation will be followed on the metal oxide phase, and the results will be compared to those obtained on a hybrid metal oxide and zeolite material. The main advantage of the hybrid material is in facilitating the desorption of CH_3O^* species through their migration from the metal oxide phase to the zeolite phase. This effect was, for

https://doi.org/10.1021/acs.energyfuels.4c03013
Energy Fuels 2024, 38, 18265−18291

example, reported for mixed ZnAlOx/H-ZMS-5, where the desorption (or dissociation) of the CH_3O^* species was facilitated, allowing their conversion into olefins over HZSM-5, via methanol or DME as intermediates. Several other reports have reported the same effect, for example the work of Tan et al. on the core−shell FeZnZr-ZSM-5 and FeZnZr-T-ZSM-5 catalysts and the work of Wang et al. on the use of ZnZrOx and ZSM-5.[44,72] In a further step, the aromatization of the produced olefins occurs in the micropores of HZSM-5.[69] However, there was no clear follow-up of the mechanism for studying the formation of aromatics. Similar findings were reported for the physically mixed ZnZrOx and ZSM-5 catalyst.[72] An additional advantage reported for this physically mixed ZnAlOx/H-ZMS-5 catalyst was the selective poisoning of the external acid sites of the zeolite by the oxide, which is generally responsible for the hydrogenation of the olefins. This was supported by the adsorption of 2,6-di-*tert*-butyl-pyridine (a bulky base probe that selectively interacts with external acid sites without being able to access the inner channels of ZSM-5). Li et al. established an elaborated mechanistic study for the CO_2 hydrogenation to aromatics over a hybrid ZnZrOx/ZSM-5 catalyst, as summarized in Figure 14.[63] Using DRIFTS, the

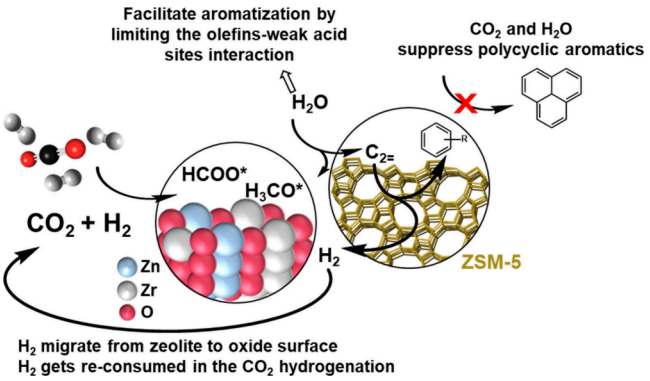

Figure 14. Insights on the tandem CO_2 hydrogenation to aromatics over a physically mixed ZnZrOx/ZSM-5 catalyst. Adapted with permission from ref 63. Copyright 2019 Elsevier.

authors also reported a decrease in the intensity of the peaks of CH_3O^* species on the ZnZrOx surface, implying their transfer onto the zeolite surface. The ease of migration of the CH_3O^* species from the oxide surface onto the zeolite is a key parameter to enhance the selectivity toward the formation of aromatics in ZSM-5 zeolite, which explains the higher selectivity of the hybrid catalyst (with the highest contact surface between the oxide and the zeolite) in comparison to the granules of mixed oxide-zeolite. Furthermore, mass spectrometry was used to compare the product distributions during the hydrogenation of CO_2 over ZnZrOx/ZSM-5 and MTO over HZSM-5. The results show that ethylene, propane, and methanol are first formed in both reactions. The formation of aromatics was noticed earlier in the case of CO_2 hydrogenation, suggesting that the CH_3O^* species (and not methanol) are the main active intermediates in the hybrid catalyst. Another advantage of the tandem process over the MTO was the formation of H_2O during the reaction, which seems to be involved in increasing the selectivity toward aromatics. To clearly understand the role of H_2O, a cofeed of ethylene-H_2O was added over ZSM-5, and the results show that the presence of a moderate amount of H_2O facilitates the conversion of light olefins to aromatics (by a factor of almost 1.8). This behavior was explained by the competitive adsorption of H_2O and ethylene on the weak acid sites, which are prone to hydrogenation and isomerization reactions. The saturation of the weak acid sites by adsorbed H_2O molecules favors the conversion of ethylene over the strong acid sites, leading to aromatics. Another important parameter is the generation of surface hydrogen species during the aromatization of olefins over ZSM-5. These latter can slow the aromatic production in the sole MTA. Luckily, in the tandem process, the generated hydrogen species are believed to migrate to the oxide−zeolite interface, where they will be consumed by the metal oxide in the CO_2 hydrogenation step. However, no mechanistic proof was established. It was also observed that the presence of CO_2 and H_2O in the feed suppresses the formation of polycyclic aromatics, typically responsible for catalyst deactivation in MTA (Figure 14).[63] The low deactivation rate during the CO_2 hydrogenation to aromatics in comparison to sole MTA was also reported by other research groups using bifunctional catalysts (e.g., Wang et al. using Cr_2O_3/ZSM-5).[68]

The selectivity toward aromatics can also be improved by tuning the location of the active acid sites in the zeolite. In that sense, Wang et al. designed a core−shell structured zeolite capsule catalyst where the outer surface acid sites (responsible for undesirable alkylation, hydrogenation, and isomerization) were passivated by a nonacidic silicalite-1. The zeolite was mortar mixed and pressed with Cr_2O_3 prior to its use in the tandem conversion of CO_2 to aromatics. The DRIFTS measurements on pure Cr_2O_3 and the bifunctional catalyst show that the HCOO* species almost disappeared in the bifunctional catalyst. Instead, peaks corresponding to CH_3O^* at 1045 cm^{-1} and C−O−C at 1211 cm^{-1} appeared, indicating the formation of methanol and ethers on the zeolite. Moreover, the vibrational peaks from the benzene ring skeleton (at 1644 cm^{-1}) and the ramifications on the ring (801 cm^{-1}) were also observed, confirming the formation of aromatics in the presence of ZSM-5 zeolite.[68] The performance of the dual catalyst was superior to the single HZSM-5 (tested in MTA), which is in accord with the results obtained by Li et al. suggesting that the migration of the formed hydrogen from olefins aromatization is the rate-limiting step for the formation of aromatics from olefins on the zeolite.[63,68] Thus, the enhanced proximity between the metal oxide and the zeolite will lead to a higher selectivity toward aromatics by increasing the hydrogen migration but also by easing, in the first step, the diffusion of the CH_3O^* species from the oxide to the zeolite surface. The impregnation of metal oxide on the zeolite surface can thus be suggested as a method to increase the intimacy of the two catalysts. However, the random dispersion of the metals on the zeolite surface may reduce the diffusion into the zeolite pores or even block the inner acidity which can be translated in the formation of light hydrocarbons and isomerization products. Controlling the zeolitic acid site density, location, and strength plays a big role in defining the product's distribution. It is known that the relatively strong acid sites are beneficial for aromatics formation. Wang et al. noticed that the aromatics selectivity increased over the bifunctional catalyst Cr_2O_3/HZSM-5 with higher Si/Al ratios (higher local acid strength). On the other side, an excessive number of acid sites is linked with the overhydrogenation of light olefin intermediate. The accessibility level of the acid sites is also primordial. The highly exposed acid sites (external surface) favor undesirable alkylation, hydrogenation, and

https://doi.org/10.1021/acs.energyfuels.4c03013
Energy Fuels 2024, 38, 18265−18291

isomerization reactions, while the internal sites (into the micropores) are believed to boost the formation of aromatics. It is also considered that the formation of aromatics in HZSM-5 follows a hydrocarbon pool mechanism, where methanol intermediates are first converted into light olefins (possibly on both external and internal sites). These species will later follow successive oligomerization, cyclization, and dehydrogenation to produce aromatics in the inner porosity.[60,106] The proximity of the external/internal acid sites, as well as the influence of site accessibility, can still benefit from a better in-depth analysis, which can be performed by the adsorption of basic probes with increased molecular size (to evaluate the accessibility index of the various types of acid sites) or by selectively poisoning the external acidity prior to catalytic tests.[69,107−109]

In summary, the tandem conversion of CO_2 to aromatics should meet the following points: (a) a sufficient amount of methanol (and thus methanol synthesis catalyst) for the following MTA process; (b) an appropriate distance between the two active sites to facilitate the migration of the methoxy species to the zeolite and the backward migration of the produced hydrogen in the zeolite to the oxide; and (c) zeolite acid sites with suitable amount, strength, location, and accessibility.[60,68] The zeolite topology remains an important factor in defining the nature of the products between aromatics (acid sites in suitable channels of ZSM-5) or longer chain hydrocarbons, e.g., C_{5+} (FAU, BEA, and also ZSM-5).[60,64,65,95]

Tan and co-workers made several attempts to produce gasoline from hydrogenation. In their first work, a hybrid FeZnZr/HY catalyst was used, and several catalytic tests were performed in order to gain insights into the formation mechanism of isoalkanes.[95] When performing the CO_2 hydrogenation reaction on FeZnZr/HY, a majority of iso-C_4 (selectivity ≈ 42%) and iso-C_5 products (21%) were obtained with partial formation of C_1 to C_4 linear alkanes. Similar hydrocarbon distribution was obtained when feeding methanol instead of CO_2 ($S_{iso\text{-}C4}$ ≈ 36% and $S_{iso\text{-}C5}$ ≈ 18%) which implies the formation of hydrocarbons by the conversion of methanol. Interestingly, the sole HY catalyst shows a lower selectivity of isoalkanes in comparison to the FeZnZr/HY composite, which indicates that FeZnZr is not limited to methanol synthesis but also contributes to the formation of isoalkanes, but no additional explanation on the role of FeZnZr was given.[95] It may be suggested that FeZnZr helps in consuming the formed hydrogen species (from olefins dehydrogenation), allowing their easier migration from the zeolite to the oxide surface.[63] Or else, this can be attributed to the difference in reactivity between the methanol and methoxy species, when these latter are formed on the surface of the metal oxide. A relationship between the increase in the isoalkanes selectivity (iso-C_4 and iso-C_5) and the decrease in the selectivity of C_2 and C_3 linear alkanes suggests that iso-C_4 is formed from the reaction of a linear C_3 with methanol through MTG reaction while iso-C_5 is formed via the additive dimerization of C_2 and C_3, a typical acid-catalyzed reaction that can take place on the zeolite (Figure 15).

Further, a core−shell FeZnZr-zeolite catalyst was prepared, which, in comparison to conventional mechanical mixed catalysts, showed improved isoalkane production from CO_2, possibly due to increased confinement in the reaction space. The confined reaction space can effectively control the consecutive secondary reactions of the intermediate species, especially in the presence of the appropriate zeolite shell size

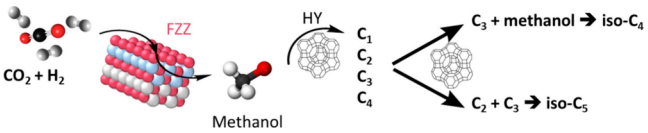

Figure 15. Proposed reaction pathway to produce isoalkanes from CO_2 hydrogenation over a FeZnZr/HY catalyst. Adapted with permission from ref 95. Copyright 2007 Elsevier.

and acid site density. The authors found that BEA zeolite favors the generation of iso-C_4 while the ZSM-5 zeolite favors the iso-C_{5+} components. The reasons were explained by different hydrocarbon formation mechanisms on both topologies. Over BEA zeolite, the formation of ethylene and propylene occurs through the aromatic side-chain mechanism while ZSM-5 zeolite favors the paring mechanism, where 1,2,4,5-tetramethylbenzene is the predominant aromatic precursor.[110−112] In Figure 16 we show the proposed mechanism for the production of ethylene and propylene from 1,2,4,5-tetramethylbenzene following (1) the pairing mechanism and (2) the side-chain mechanism. Other alternative mechanisms were also reported in the literature and are also reported in Figure 16, such as (3) the paring-type mechanism and (4) the ring-expansion mechanism. Mechanism 3 is the only mechanism that does not involve a methylation step since the ring contraction occurs after a simple protonation step. For all of the other mechanisms, the methylation step is required (carbon from the methylation step is shown in red). After the methylation step, the paring mechanism follows a ring contraction to a five-membered ring. As a result, ethyl or isopropyl groups are formed and are subsequently cracked into ethylene or propylene, respectively. Both molecules contain one carbon from the aromatic ring. The side-chain mechanism is also initiated by a methylation step, which is in this type of mechanism followed by a deprotonation, resulting in the formation of an exocyclic double bond. Further methylation steps can take place on the exocyclic double bond to form a side chain that can crack into ethylene (after one additional methylation) or propylene (after two additional methylations). Finally, the ring expansion is also initiated by methylation which is followed by the ring expansion. After isomerization steps, alkyl ramifications are formed and eliminated. The produced ethylene or propylene contains one aromatic ring carbon, similarly to the pairing mechanism.[110−112] The following mechanism majorly affects the final products. If assuming that ZSM-5 follows the pairing mechanism, the formation of propylene can thus be favored over ethylene, leading to iso-C_{5+} products by the oligomerization of propylene with C_2 or larger olefin products. On the other hand, the side-chain mechanism (favored over BEA zeolite) may favor ethylene production over propylene, which, after oligomerization, produces iso-C_4 (ethylene + ethylene).[106,111] The combination of two zeolite topologies was shown to improve the selectivity toward isoproducts, where high yields of iso-C_4 and iso-C_{5+} were obtained with double-zeolites shell catalyst (ZSM-5/BEA and ZSK-5/HY). This high performance was attributed to the synergetic effect between the zeolite topologies; however, no additional mechanistic understanding was given, mainly due to the complexity of the system.[96]

In a more recent work, Tan et al. further improved the production of gasoline from CO_2 hydrogenation over a core−shell FeZnZr@ZSM-5 catalyst by optimizing the amount of

https://doi.org/10.1021/acs.energyfuels.4c03013
Energy Fuels 2024, 38, 18265−18291

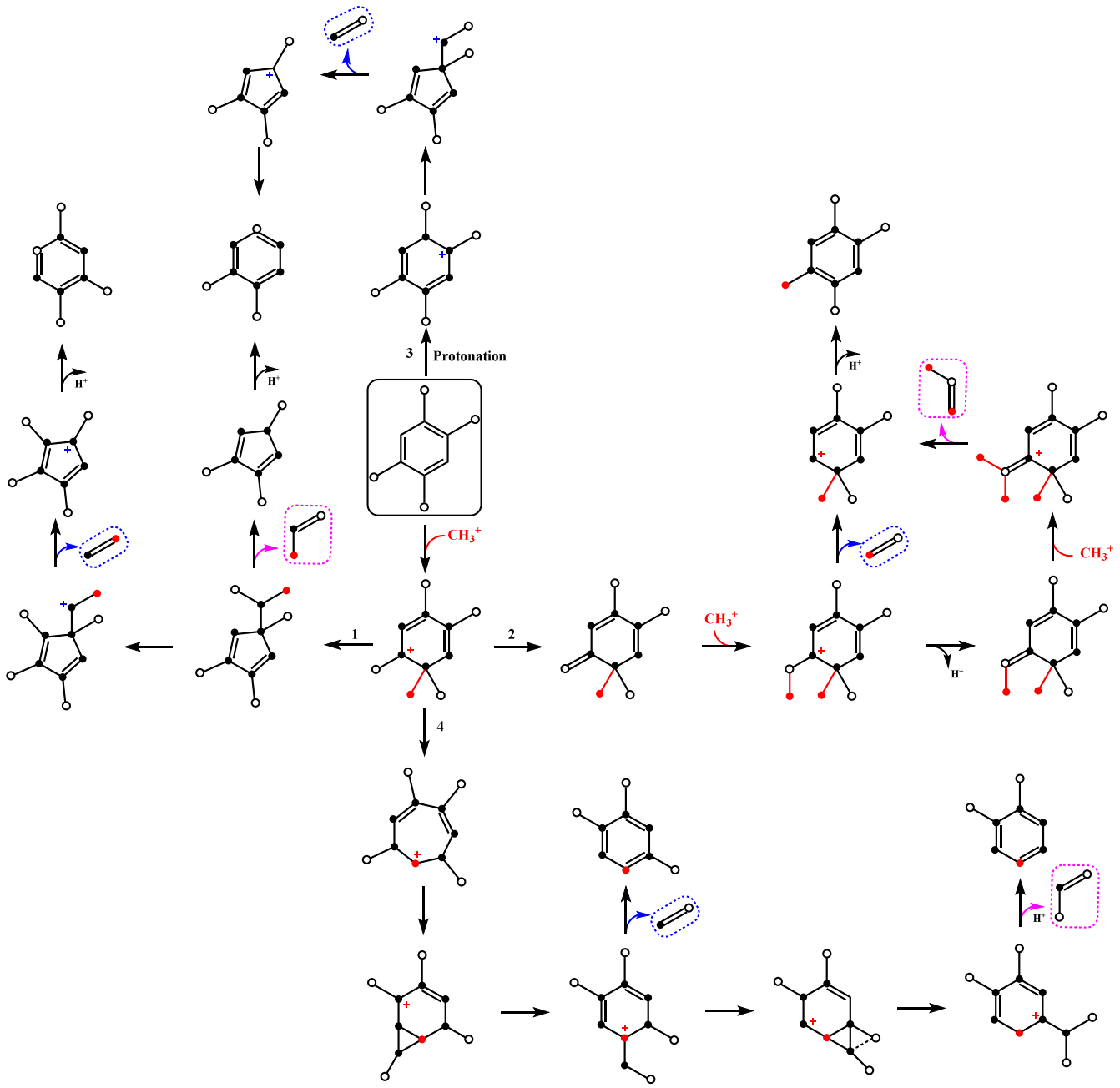

Figure 16. Summary of proposed mechanisms to produce ethylene and propylene from 1,2,4,5-tetramethylbenzene (a model aromatic compound). The different paths represent different mechanisms. From 1 to 4, the mechanisms are (1) the paring mechanism, (2) the side-chain mechanism, (3) the protonation mechanism or the paring-type mechanism, and (4) the ring-expansion mechanism. The colors of the carbon atoms represent their origin in the mechanism: black (aromatic ring carbon), white (methyl ramification in 1,2,4,5-tetramethylbenzene), and red (methyl groups from the methylation step). Adapted with permission from ref 111. Copyright 2014 Elsevier.

Bronsted acid sites and the thickness of the zeolite shell.[113] The acid strength was estimated on the FeZnZr core using NH_3-temperature programmed desorption (TPD) where weak and medium acid sites are observed (broad peak between 100 and 450 °C). However, the ones presumed desired for methanol conversion (strong acid sites) were not detected.[96,114] The NH_3-TPD profiles on a series of FeZnZr@ZSM-5 core−shell catalysts with different FeZnZr/zeolite ratios show that the density of strong Bronsted acid sites increases with the increase in the fraction of zeolite. However, an excessive amount of sites enhances the hydrocracking of the long-chain hydrocarbons and the hydrogenation of lower olefins, which results in a drop in the selectivity to gasoline. Next to controlling the acid density, the thickness of the zeolite shell affects the contact time of the reactants and intermediates with the inner zeolite acidity. The zeolite shell only becomes effective from a certain thickness, where a thin shell will limit the contact time between methanol and the zeolitic acid sites, leading to no beneficial effect. On the other hand, a large zeolite shell will enhance the production of aromatics by the high abundance of acid sites. The adequate thickness of the shell will lead to a higher C_{5+} selectivity; however, this will also be dependent on the used GHSV.

https://doi.org/10.1021/acs.energyfuels.4c03013
Energy Fuels 2024, 38, 18265−18291

Table 6. Possible Reactions on the CTM and MTH Sides of the Methanol-Mediated CO_2 to Hydrocarbons Reaction

Reaction no.	Description	Reaction
	Reactions on the CTM Side	
1	CO_2 hydrogenation to methanol	$CO_2 + 3H_2 \leftrightarrow CH_3OH + H_2O$
2	Reverse water−gas shift	$CO_2 + H_2 \leftrightarrow CO + H_2O$
3	CO hydrogenation to methanol	$CO + 2H_2 \leftrightarrow CH_3OH$
4	Methanation of CO	$CO + 3H_2 \leftrightarrow CH_4 + H_2O$
5	Methanation of CO_2	$CO_2 + 4H_2 \leftrightarrow CH_4 + 2H_2O$
	Reactions on the MTH Side	
6	Methanol to ethane	$2CH_3OH + H_2 \rightarrow C_2H_6 + 2H_2O$
7	Methanol to propane	$3CH_3OH + H_2 \rightarrow C_3H_8 + 3H_2O$
8	Methanol to butane	$4CH_3OH + H_2 \rightarrow C_4H_{10} + 4H_2O$
9	Methanol to ethylene	$2CH_3OH \rightarrow C_2H_4 + 2H_2O$
10	Methanol to propylene	$3CH_3OH \rightarrow C_3H_6 + 3H_2O$
11	Methanol to butylene	$4CH_3OH \rightarrow C_4H_8 + 4H_2O$
12	Autocatalytic growth of ethylene from methanol	$C_2H_4 + 2CH_3OH \rightarrow 2C_2H_4 + 2H_2O$
13	Autocatalytic growth of propylene from methanol	$C_3H_6 + 3CH_3OH \rightarrow 2C_3H_6 + 3H_2O$
14	Autocatalytic growth of butylene from methanol	$C_4H_8 + 4CH_3OH \rightarrow 2C_4H_8 + 4H_2O$
15	Ethylene hydrogenation to ethane	$C_2H_4 + H_2 \rightarrow C_2H_6$
16	Propylene hydrogenation to propane	$C_3H_6 + H_2 \rightarrow C_3H_8$
17	Butylene hydrogenation to butane	$C_4H_8 + H_2 \rightarrow C_4H_{10}$
18	C_{5-8} formation from ethylene (oligomerization reaction)	$C_2H_4 \rightarrow 0.307C_{5-8}$
19	C_{5-8} formation from propylene (oligomerization reaction)	$C_3H_6 \rightarrow 0.461C_{5-8}$
20	C_{5-8} formation from butylene (oligomerization reaction)	$C_4H_8 \rightarrow 0.615C_{5-8}$
21	C_{5-8} cracking to ethylene	$0.307C_{5-8} \rightarrow C_2H_4$
22	C_{5-8} cracking to propylene	$0.461C_{5-8} \rightarrow C_3H_6$
23	C_{5-8} cracking to butylene	$0.615C_{5-8} \rightarrow C_4H_8$
24	C_{9+} formation from ethylene and C_{5-8}	$C_2H_4 + C_{5-8} \rightarrow 0.809C_{9+}$
25	C_{9+} formation from propylene and C_{5-8}	$C_3H_6 + C_{5-8} \rightarrow 0.904C_{9+}$
26	C_{9+} formation from butylene and C_{5-8}	$C_4H_8 + C_{5-8} \rightarrow C_{9+}$

From this study, we conclude that the methanol (or DME) coming from the oxide phase will be converted on the Bronsted acid sites of the zeolite (shell) to first form light hydrocarbons (C_2−C_4). These latter will follow a cascade polymerization, isomerization, and hydrogen transfer reaction to make C_{5+} gasoline product range products. An appropriate amount of BAS and shell thickness are needed to enhance the C_{5+} formation.[98,106,115−120] The excessive amount of BAS can cause the undesired production of light alkanes either by hydrogen transfer of the light C_2−C_4 olefins or by the cracking of longer hydrocarbon chain molecules.[113]

3.6. Modeling of the Tandem System. Studying the kinetics of the tandem catalytic system of the methanol-mediated CO_2 to hydrocarbons reaction creates multiple challenges as it is not sufficient to simply combine the kinetics of the different steps, but it implies one should consider the way each rate is influenced by the others.

To start with, Sharma et al. have highlighted various kinetic studies for the CTM reaction using both noble and non-noble metal catalysts.[7] Primarily, Cu-based systems have been explored for metal-catalyzed methanol synthesis. For instance, Graaf et al. developed Langmuir−Hinshelwood−Hougen−Watson (LHHW) kinetics for low-pressure methanol synthesis over a CuZnAl catalyst, indicating that methanol can be produced from both CO and CO_2, coupled with dissociated hydrogen.[121] Diaz et al. proposed an LHHW model with a three-site adsorption mechanism over a PdCuZn/SiC catalyst, identifying formate hydrogenation as the rate-determining step.[122] Similarly, Grabow and Mavrikakis introduced microkinetic models using $Cu/ZnO/Al_2O_3$ catalyst that integrate multiple reaction intermediates and byproducts such as HCOOH*, CH_3O_2*, formic acid, formaldehyde, and methyl formate.[123] Frei et al.[124] developed a microkinetic model for CTM over In_2O_3, while Hus et al.[125] described a mean-field microkinetic model encompassing 33 reversible elementary steps for CTM kinetics over various metallic catalysts.

The kinetics of the MTH reaction are complex and have been extensively studied, particularly with ZSM-5 and SAPO catalysts focusing on olefin production (MTO). However, recent studies, as reviewed by Ghosh et al.,[126] have also considered the production of higher hydrocarbons from methanol. Park et al. created a kinetic model for the MTO reaction using an HZSM-5 catalyst, attributing primary olefin formation to the surface oxonium ylide mechanism and higher olefin formation to the carbenium ion mechanism.[127] Kaarsholm et al. proposed a hydrocarbon pool mechanism

https://doi.org/10.1021/acs.energyfuels.4c03013
Energy Fuels 2024, 38, 18265−18291

model with 15 primary reaction steps, explaining olefin generation through reversible reactions over a phosphorus-modified ZSM-5 catalyst, with high molecular weight hydrocarbons forming alongside olefins within the catalyst pores.[128] Aguayo et al. developed a kinetic model featuring seven product lumps for MTO over HZSM-5 at 400−500 °C.[129] Kumar et al. demonstrated that DME and primary olefins form via an aromatic hydrocarbon pool, with higher olefins forming through an alkene homologation cycle.[130] Ryu et al. proposed nine reactions based on the hydrocarbon pool mechanism, resulting in lower paraffins, olefins, and C5+ hydrocarbons using SAPO-34 for MTO.[131]

Conversely, limited literature exists on the kinetic modeling of direct hydrogenation of CO_2 to hydrocarbons mediated by methanol with a tandem catalytic system. According to Sharma et al.,[7] tandem approaches result in higher activity rates and selectivity (versus pure CTM and MTH) due to the synergistic effects. For example, as already mentioned, it has been suggested that a Cr_2O_3/HZSM-5 mixture facilitates surface diffusion of methanol intermediates from the oxide to the zeolite, enhancing overall performance.

The full list of possible reactions linked to the CTM and the MTH of the methanol-mediated CO_2 to hydrocarbons reaction modeling used by the only two studies found on the topic (Cordero-Lanzac et al. and Ghosh et al.[126]) are detailed in Table 6.

Cordero-Lanzac et al. presented an LHHW kinetic model for the direct hydrogenation of CO_2 to light hydrocarbons (up to C4) using a PdZn/ZrO_2 + SAPO-34 catalyst.[132] This model includes reactions 1−4 (on the metal alloy/oxide side) and 6−8 (on the SAPO-34 side) from the showcased set in Table 6. This model assumes that methanol is converted to ethylene, propylene, and butenes over the SAPO-34. Afterward, the high partial pressure of H_2 and the Pd in the catalyst results in the fast hydrogenation of olefins to ethane, propane, and butanes.

The study evaluated the performance of a three-layer reactor, configured with 10% of the bed containing CTM catalyst, 80% with a 1:1 mixture of catalysts, and the remaining 10% with MTH catalyst versus mixed and dual bed configurations. The three-layer reactor achieved conversion levels similar to those of the mixed bed configuration and higher than those of the dual bed configuration. In all configurations, the simulated CO_2 conversion and product distribution closely matched experimental observations under various process conditions. However, the kinetic model developed for the study assumed steady-state conditions and did not account for catalyst deactivation, as it was based on laboratory-scale observations, indicating potential areas for further improvement.

The study by Ghosh et al. proposes an LHHW kinetic model for the direct hydrogenation of CO_2 to hydrocarbon products, including the gasoline range and, e.g., a C9+ lump, over an In_2O_3/HZSM-5 bifunctional catalytic bed. This model integrates an LHHW-based reaction mechanism for the hydrogenation of CO_2 to methanol over the In_2O_3 catalyst with a lumped MTH model over the HZSM-5 zeolite. The MTH model was adapted from the kinetic model for the conversion of DME to olefins over HZSM-5 zeolite, developed by Perez-Uriarte et al.[133] This model includes reactions 1−2 and 5 (on the In_2O_3 side) and 9−26 (for the HZSM-5 side) from the showcased set in Table 6.

It is important to note that this model does not include DME as an intermediate in the conversion from methanol to hydrocarbons, despite it being a key component in the Perez-Uriarte et al. lump model used as a reference. Ghosh et al. determined that incorporating DME-related reactions had a minimal impact on fitting the experimental data. Additionally, DME was not detected experimentally, suggesting that it is consumed too rapidly to be observed as an intermediate in the formation of hydrocarbons.

Compared to the Cordero-Lanzac et al. model, the Ghosh model incorporates a more extensive reaction network and achieves the production of higher hydrocarbons. It implements CO_2 as the precursor of methane instead of CO and considers the intermediate transformation of methanol into olefins. It also effectively captures the suppression of the rWGS reaction and demonstrates how variations in catalyst mass ratios can influence methanol output and selectivity toward higher hydrocarbons. Additionally, the model shows a higher hydrocarbon yield compared with the indirect CO_2 hydrogenation route (so CTM + MTH), evidencing the relevance of tandem catalysis.

However, there is room for improving the Ghosh model. The prediction accuracy for methanol and CO production in the CTM section is not as high as that for other products. Integrating a more comprehensive model for the CTM section such as the one developed by Frei et al., which achieves errors within the 0.15 range, could enhance the accuracy. Ghosh et al. also suggests that inaccuracies may arise from using the exact kinetic parameters for CH_3OH, CO, and CH_4 formation from a previous study by Ghosh et al. (2021), which focused solely on the CTM section.[134] Refitting the kinetic parameters within the tandem context is necessary. On a similar note, the model does not fully account for the inhibiting effects due to higher concentrations of water and hydrocarbons on the CTM sites nor the effects of high concentrations of CO_2 and H_2 on the MTH sites. Better performance of the model could also be achieved by integrating aromatics as separate components instead of lumping them together. Finally, regarding catalyst stability, the modeling study by Ryu et al. addressed important factors such as coke formation and deactivation for SAPO-34 and this could be adapted for the HZSM-5 catalyst used by Ghosh.

4. OUTLOOK AND PRACTICAL INSIGHTS

In the present day, there is no clear understanding of the mechanism of combined CTM and MTG in one step using tandem catalytic systems. There is a clear need for more uniformity in research methodologies as well as in the way results are presented or plotted in order to safely compare catalysts or conditional changes and infer safe conclusions. Along with temperature and pressure, the GHSV is obviously the most important condition in such systems, and thus a clear mentioning is demanded, along with details on how it was calculated based on real reactor inputs. In addition, it is essential for results to be translated in space time yields and conversions in order to compare systems at different GHSVs. In the same perspective, it is important to report and plot selectivity on a carbon basis and not only on a hydrocarbon basis to avoid misleading information especially when the conversion is low and the carbon balance is not 100%. The carbon balance issue indicates that the "missing" carbon can be relatively high compared to the amount of carbon that is converted, and this is often overlooked. The hydrocarbon basis often embellishes results or allows one to highlight smaller differences, but one can ask what the point is if the catalyst

https://doi.org/10.1021/acs.energyfuels.4c03013
Energy Fuels 2024, 38, 18265−18291

makes over 70% of CO. From this perspective, ways to decrease the CO content of the final product need to be studied in such systems. It has been proven that the addition of CO in the feed, or the recycling of it from the output of the reactor, works beneficially to suppress the unwanted rWGS reaction, but only few researchers have included the CO cofeeding technique in the systems that are discussed. At the same time it was observed that no variations of pressure were studied for specific systems, and our recommendation is to test at least a high- and a low-pressure regime. In parallel, when different temperatures are tested for a system, it is deemed critical to present the same temperature testing for the CTM part alone, due to the fact that higher temperatures could lead to higher selectivity toward CO resulting in a higher yield of gasoline through a different, additional route. This could help researchers understand better the mechanistic route that is being followed and consequently enhance the product production through one particular pathway. The CTM part of the tandem systems always needs to be presented as a comparison and clarification of the route that is being followed. When reporting STX and STY of a CTM catalyst in order to compare its role in the tandem, it is advisible to make sure the weight of catalyst (g) basis is adjusted: i.e., the oxide part in a 1:1 tandem where STX is reported is actually converting twice the amount of CO_2 per unit of time on an oxide weight basis.

Nowadays, a lot of effort is being made to synthesize complex bifunctional systems especially for integrating the CTM part on, in, or underneath a zeolite part (e.g., core−shells). However, the stability of these systems and the possibility of using them at larger scales in industrial conditions need to be taken into account since most of the times such systems lack efficiency and present tedious and expensive synthesis methods unfit for scaling up. In such complex catalyst designs, long-term stability (on stream and in repetitive regeneration) also remains questionable. In that sense, separate dual component systems working in tandem might offer a better perspective.

Moreover, in such coupled systems, research still needs to be done on how the materials are best geometrically placed inside the reactor and how this affects their interaction. There is a lot of space and need to further investigate the effects of proximity and catalyst bed configuration. In some cases, the proximity had a detrimental effect on the reaction, while on others, the opposite was seen. It is important to understand what the main mechanistic factors are that influence the tandem system both chemically, physically (mass transport), and heat-wise, in particular when altering the proximity of the materials. Reasoning about the beneficial role of particular configurations without considering these fundamentals would not improve the total understanding of the coupled catalyst and its functioning in a gaseous reactor.

On the mechanistic side, it would be of great importance to compare, with a standard protocol, the shift in the IR peaks of the intermediate species for the different oxides. Later, it would be useful to link this shift to the strength of interaction of these intermediates with the surface (adsorption energies, ease of desorption, and rate-determining steps) in order to correlate it to the catalytic performances. More care could also be given to the stability of the intermediates on the surface, which translates into their activation and desorption rates. Recently, this was found to affect the rate-determining step of CO_2 hydrogenation, leading to variations in the reaction pathways. For the tandem process, the study of MeOH adsorption of the oxide and zeolite catalysts may deliver a better understanding of the migration of methanol (or methoxy species). A high affinity toward MeOH is needed for the used zeolites, yet the excessive interaction may lead to lower MeOH conversion or enhanced coke formation. Integrating a more comprehensive kinetic model for the CTM section, which achieves errors within a low range, could enhance the robustness and scalability of the process design. Models for tandem catalysis should be improved or developed de novo, with coke formation and catalyst deactivation integrated into the kinetics.

It is crucial to mention that up to this date no research has focused on producing a drop-in gasoline directly from CO_2 through methanol, and this is because most work targets specific products (aromatics, alkanes, olefins, etc.) and not a blend of hydrocarbons that would be a directly acceptable product itself. Such a work or focus could open many possibilities in the field; however, the challenges to overcome are many, especially if the goal is a product that meets the official qualifications for an engine fuel. Easily blendable fractions could also be considered. In the future the demand for hydrocarbon blends with specific properties may be seen as a relevant target for CO_2 reuse pathways.

Beyond gasoline, research efforts are also targeting the production of other fuels, for instance, sustainable aviation fuels (SAFs), which are gaining more and more attention as part of global goals to reduce CO_2 emissions. In particular, e-SAFs (SAFs deriving from CO_2 and electricity through the methanol or FT pathway) have seen large investments from international companies globally for plants to be functional before 2030. Methanol-derived jet fuels are the basis for many of these investments; however, many challenges remain due to the complexity of these chemical routes. Among others, due to the fact that by targeting specific blends, significant byproducts (e.g., LPG) are expected in a similar way as in the MTG process.[135] This statement reinforces the need for dedicated scientific studies on the development of catalysts and processes for the conversion of CO_2 to fuels via the methanol route.

5. CONCLUSIONS

CO_2 conversion to MeOH followed by MTG in one step over a tandem system is a very challenging topic due to the multiple reactions occurring at the same time with direct influence over each other. Choosing the right catalytic materials for each reaction and at the same time combining them in the right way by altering the ratio of the catalysts or the configuration of the catalytic bed are of high importance, and some research has been done in this direction with ZnZrOx being the most highlighted oxide for CTM and ZSM-5 being the most researched zeolite for MTG/MTA. Additionally, the conditions at which such coupled processes occur and the frequency of their usage have been investigated here, in order to draw relations with product profiles, as they can enhance or minimize the yields of desired products or shift the reaction in different directions. The areas that lack understanding and need further investigation have been underlined as well as the directions and practical guidelines which researchers could follow to obtain useful data (i.e., allowing easy verification and comparison) on such complicated systems. Overall, it cannot be safely concluded what the effect of increasing temperature at a given pressure is because even though there is an increase in the STY of desired products, there is no clear evidence that this is indeed due to the temperature effect or the alteration of the mechanism of the

https://doi.org/10.1021/acs.energyfuels.4c03013
Energy Fuels 2024, 38, 18265−18291

reactions. As for the pressure, no clear comparisons under different pressures were made while keeping the rest of the parameters stable. For these reasons it was necessary to study the mechanistic aspects of such systems as the mechanism can show such shifts between FTS or CTM combined with MTG or explain the prevalence of classes of products (aromatics vs light olefins, e.g.). IR spectroscopy is widely used in studying the mechanism of CO_2 hydrogenation, and several mechanistic insights were extracted mainly by determining the reactions intermediates (formate and methoxy species). However, the comparison between different oxides must be made with a standard protocol, which is lacking to date. It would be of great importance to compare the shift in IR peaks to the strength of the interaction of the intermediates and, later, to the catalytic performances. Kinetics of these systems are also a challenging topic, as the prediction accuracy for methanol and CO production in the CTM section is not as high for other products. It has been suggested that inaccuracies may arise from using the exact kinetic parameters based on studies that focused solely on the CTM section. Refitting the kinetic parameters within the tandem context is necessary. Overall, more research needs to be done to obtain a deeper comprehension of how tandem systems work if one truly desires high STXs and STYs to coincide. The future perspectives and challenges were discussed in detail, leading to a key conclusion that more specific investigations into the direct synthesis of drop-in capable gasolines or (e-)SAFs need to be addressed in order to obtain realistic fuels closer to the desired qualifications of the industry at the moment.

■ ASSOCIATED CONTENT

Supporting Information

The Supporting Information is available free of charge at https://pubs.acs.org/doi/10.1021/acs.energyfuels.4c03013.

Additional details on vibrational frequencies of infrared peaks for surface species over reported metal oxides (PDF)

■ AUTHOR INFORMATION

Corresponding Authors

Grégoire Léonard − *Department of Chemical Engineering, Université de Liège, 4000 Liège, Belgium*; Email: g.leonard@uliege.be

Michiel Dusselier − *Center for Sustainable Catalysis and Engineering (CSCE), KU Leuven, 3001 Leuven, Belgium*; orcid.org/0000-0002-3074-2318; Email: michiel.dusselier@kuleuven.be

Authors

Foteini Lappa − *Center for Sustainable Catalysis and Engineering (CSCE), KU Leuven, 3001 Leuven, Belgium*

Ibrahim Khalil − *Center for Sustainable Catalysis and Engineering (CSCE), KU Leuven, 3001 Leuven, Belgium*; orcid.org/0000-0003-0263-1079

Alejandro Morales − *Department of Chemical Engineering, Université de Liège, 4000 Liège, Belgium*

Complete contact information is available at: https://pubs.acs.org/10.1021/acs.energyfuels.4c03013

Notes

The authors declare no competing financial interest.

Biographies

Foteini Lappa is a joint Ph.D. student in the Center for Sustainable Catalysis and Engineering, KU Leuven and in the Department of Chemical Engineering, Université de Liège, in Belgium. Her Ph.D. research work focuses on CO_2 conversion to hydrocarbons. Her integrated M.Sc. degree was obtained after studying the catalytic conversion of bioglycerol toward high added value chemical feedstocks, at the Laboratory of Petrochemical Technology, Chemical Engineering, Aristotle University of Thessaloniki (AUTh), Greece, (2021).

Dr. Ibrahim Khalil (Ramieh, Lebanon) obtained his Bachelor's degree in Chemistry at Lebanese University (2013) and his Master's in Environmental Chemistry at University of Poitiers (2015). In 2018, he obtained his Ph.D. in analytical and physical chemistry from Laboratory Catalysis and Spectrochemistry, developing a purification process for second-generation biofuels. Since 2019, he has joined the Dusselier lab at KU Leuven as a postdoctoral researcher, developing metal on zeolite catalysts and FT-IR spectroscopy methods.

Alejandro Morales is a Chemical Engineer from Los Andes University in Colombia. He has a M.Sc. in Project Management for Environmental and Energy Engineering from IMT Atlantique in France. He is finishing his Ph.D. at the Chemical Engineering department of the University of Liege in Belgium as part of Professor Gregoire Leonard's team. His research focuses on the sustainable production of Fischer−Tropsch fuels.

Prof. Grégoire Léonard, Faculty of Applied Sciences, Chemical Engineering, University of Liège, focuses on Process System Engineering applications for the chemical and energy industrial sectors. After obtaining degrees in Chemical Engineering (University of Liège) and Mechanical Engineering (Technical University of Munich) and defending his Ph.D., he conducted research at Columbia University and Arizona State University. He is a member of the Computer Aided Process Engineering working party and of the Energy section (EFCE), of the CO_2 Value Europe association.

Prof. Michiel Dusselier obtained his Ph.D. (Bioscience Engineering Catalytic Technology) at KU Leuven, Belgium and did postdoctoral work at Caltech, USA. He is now an associate professor at KU Leuven and cofounded the Center for Sustainable Catalysis and Engineering. His focus is on zeolite synthesis, degradable plastics, heterogeneous catalysis and CO_2 conversion. He has received the Young Researcher Award of the International Zeolite Association (2022) and the N3C Award of the Dutch Catalysis Society (2023).

■ ACKNOWLEDGMENTS

F.L., G.L. and M. D. acknowledge the main funding for this work: BE-HyFE project funded by the federal Energy Transition Fund by FPS Economy. I.K. acknowledges the FWO Foundation for the Senior postdoctoral research grant (12A3M24N). M.D. acknowledges funding from KU Leuven Grant C14/20/086. A.M. and G.L. also thank the Energy Transition Fund project PROCURA, funded by the Belgian Ministry of Economy.

■ ABBREVIATIONS

BAS, Bronsted acid sites; BET, Brunauer−Emmett−Teller; CCS, carbon capture and storage; CCU, carbon capture and utilization; CTG, CO_2 to gasoline; CTM, CO_2 to methanol; DFT, density functional theory; DME, dimethyl ether; DRIFTS, diffuse reflectance infrared Fourier transform spectroscopy; EPR, electron paramagnetic resonance; FTS, Fischer−Tropch synthesis; GHG, greenhouse gas; GHSV,

gas hourly space velocity; GWP, global-warming potential; HCs, hydrocarbons; LPG, liquefied petroleum gas; MeOH, methanol; MTA, methanol to aromatics; MTG, methanol to gasoline; MTH, methanol to hydrocarbons; MTO, methanol to olefins; rWGS, reverse water−gas shift; SEM, scanning electron microscopy; SMR, steam methane reforming; STEM, scanning transmission electron microscopy; STX, space time conversion; STY, space time yield; TEM, transmission electron microscopy; TPABr, tetrapropylammonium bromide; TPD, temperature-programmed desorption; TRL, technology readiness level; WGS, water−gas shift; XRD, X-ray diffraction

REFERENCES

(1) Erickson, L. E.; Brase, G. Paris Agreement on Climate Change. *Reducing Greenh. Gas Emiss. Improv. Air Qual.* **2019**, 11−22.

(2) Skytt, T.; Nielsen, S. N.; Jonsson, B.-G. Global Warming Potential and Absolute Global Temperature Change Potential from Carbon Dioxide and Methane Fl Uxes as Indicators of Regional Sustainability − A Case Study of Jämtland, Sweden. *Ecol. Indic.* **2020**, *110*, No. 105831.

(3) Lashof, D. A.; Ahuja, D. R. Relative Contributions of Greenhouse Gas Emissions to Global Warming. *Nature* **1990**, *344*, 529−531.

(4) Jeffry, L.; Ong, M. Y.; Nomanbhay, S.; Mofijur, M.; Mubashir, M.; Show, P. L. Greenhouse Gases Utilization: A Review. *Fuel* **2021**, *301* (April), No. 121017.

(5) Yokoi, R.; Watari, T.; Motoshita, M. Future Greenhouse Gas Emissions from Metal Production: Gaps and Opportunities towards Climate Goals. *Energy Environ. Sci.* **2022**, *15* (1), 146−157.

(6) Peres, C. B.; Resende, P. M. R.; Nunes, L. J. R.; Morais, L. C. d. Advances in Carbon Capture and Use (CCU) Technologies: A Comprehensive Review and CO_2 Mitigation Potential Analysis. *Clean Technol.* **2022**, *4*, 1193−1207.

(7) Sharma, P.; Sebastian, J.; Ghosh, S.; Creaser, D.; Olsson, L. Recent Advances in Hydrogenation of CO2into Hydrocarbonsvia-methanol Intermediate over Heterogeneous Catalysts. *Catal. Sci. Technol.* **2021**, *11* (5), 1665−1697.

(8) Hepburn, C.; Adlen, E.; Beddington, J.; Carter, E. A.; Fuss, S.; Mac Dowell, N.; Minx, J. C.; Smith, P.; Williams, C. K. The Technological and Economic Prospects for CO2 Utilization and Removal. *Nature* **2019**, *575* (7781), 87−97.

(9) Pan, S. Y.; Chiang, P. C.; Pan, W.; Kim, H. Advances in State-of-Art Valorization Technologies for Captured CO2 toward Sustainable Carbon Cycle. *Crit. Rev. Environ. Sci. Technol.* **2018**, *48* (5), 471−534.

(10) Saeidi, S.; Najari, S.; Hessel, V.; Wilson, K.; Keil, F. J.; Concepción, P.; Suib, S. L.; Rodrigues, A. E. Recent Advances in CO 2 Hydrogenation to Value-Added Products — Current Challenges and Future Directions. *Prog. Energy Combust. Sci.* **2021**, *85*, No. 100905.

(11) Niu, J.; Liu, H.; Jin, Y.; Fan, B.; Qi, W.; Ran, J. Comprehensive Review of Cu-Based CO2 Hydrogenation to CH3OH: Insights from Experimental Work and Theoretical Analysis. *Int. J. Hydrogen Energy* **2022**, *47* (15), 9183−9200.

(12) Velazquez Abad, A.; Dodds, P. E. Green Hydrogen Characterisation Initiatives: Definitions, Standards, Guarantees of Origin, and Challenges. *Energy Policy* **2020**, *138*, No. 111300.

(13) Patlolla, S. R.; Katsu, K.; Sharafian, A.; Wei, K.; Herrera, O. E.; Merida, W. A Review of Methane Pyrolysis Technologies for Hydrogen Production. *Renewable Sustainable Energy Rev.* **2023**, *181*, 113323.

(14) Katebah, M.; Al-rawashdeh, M.; Linke, P. Analysis of Hydrogen Production Costs in Steam-Methane Reforming Considering Integration with Electrolysis and CO_2 Capture. *Clean. Eng. Technol.* **2022**, *10*, No. 100552.

(15) Bhandari, R.; Trudewind, C. A.; Zapp, P. Life Cycle Assessment of Hydrogen Production via Electrolysis e a Review. *J. Clean. Prod.* **2014**, *85*, 151−163.

(16) Ji, M.; Wang, J. ScienceDirect Review and Comparison of Various Hydrogen Production Methods Based on Costs and Life Cycle Impact Assessment Indicators. *Int. J. Hydrogen Energy* **2021**, *46* (78), 38612−38635.

(17) Dincer, I.; Acar, C. ScienceDirect Review and Evaluation of Hydrogen Production Methods for Better Sustainability. *Int. J. Hydrogen Energy* **2015**, *40* (34), 11094−11111.

(18) Rojas, J.; Zhai, S.; Sun, E.; Haribal, V.; Marin-quiros, S.; Sarkar, A.; Gupta, R.; et al. Technoeconomics and Carbon Footprint of Hydrogen Production. *Int. J. Hydrogen Energy* **2024**, *49*, 59−74.

(19) Diab, J.; Fulcheri, L.; Hessel, V.; Rohani, V.; Frenklach, M. Why Turquoise Hydrogen Will Be a Game Changer for the Energy Transition. *Int. J. Hydrogen Energy* **2022**, *47* (61), 25831−25848.

(20) Korányi, T. I.; Németh, M.; Beck, A.; Horváth, A. Recent Advances in Methane Pyrolysis: Turquoise Hydrogen with Solid Carbon Production. *Energies* **2022**, *15* (17), 6342.

(21) Hermesmann, M.; Müller, T. E. Green, Turquoise, Blue, or Grey? Environmentally Friendly Hydrogen Production in Transforming Energy Systems. *Prog. Energy Combust. Sci.* **2022**, *90*, No. 100996.

(22) Molina, A.; Mondragón, F. Reactivity of Coal Gasification with Steam and CO 2. *Fuel* **1998**, *77* (15), 1831−1839.

(23) Yu, J.; Tian, F. J.; Chow, M. C.; McKenzie, L. J.; Li, C. Z. Effect of Iron on the Gasification of Victorian Brown Coal with Steam: Enhancement of Hydrogen Production. *Fuel* **2006**, *85* (2), 127−133.

(24) Fernández-González, J.; Rumayor, M.; Domínguez-Ramos, A.; Irabien, A. Hydrogen Utilization in the Sustainable Manufacture of CO2-Based Methanol. *Ind. Eng. Chem. Res.* **2022**, *61* (18), 6163−6172.

(25) Mondal, U.; Yadav, G. D. *Analysis of Catalytic Processes, Reactors And* **2021**, *23*, 8361−8405.

(26) International Renewable Energy Agency (IRENA). *Innovation Outlook: Renewable Methanol*, 2021. https://www.irena.org/publications/2021/Jan/Innovation-Outlook-Renewable-Methanol (accessed 23 January 2024).

(27) Moreno-Ruiz, E.; et al. Documentation of changes implemented in the ecoinvent database v3.10 (2023.11.28), ecoinvent Report No. 5 (v4); The ecoinvent Centre: St. Gallen, Switzerland, 2013; pp 1−138.

(28) Salahudeen, N.; Rasheed, A. A.; Babalola, A.; Moses, A. U. Review on Technologies for Conversion of Natural Gas to Methanol. *J. Nat. Gas Sci. Eng.* **2022**, *108* (April), No. 104845.

(29) Rumayor, M.; Dominguez-Ramos, A.; Irabien, A. Innovative Alternatives to Methanol Manufacture : Carbon Footprint Assessment. *J. Clean. Prod.* **2019**, *225*, 426−434.

(30) Tackett, B. M.; Gomez, E.; Chen, J. G. Net Reduction of CO2 via Its Thermocatalytic and Electrocatalytic Transformation Reactions in Standard and Hybrid Processes. *Nat. Catal.* **2019**, *2* (5), 381−386.

(31) Jiang, X.; Nie, X.; Guo, X.; Song, C.; Chen, J. G. Recent Advances in Carbon Dioxide Hydrogenation to Methanol via Heterogeneous Catalysis. *Chem. Rev.* **2020**, *120* (15), 7984−8034.

(32) Kim, H.; Byun, M.; Lee, B.; Lim, H. Carbon-Neutral Methanol Synthesis as Carbon Dioxide Utilization at Different Scales : Economic and Environmental Perspectives. *Energy Convers. Manage.* **2022**, *252*, No. 115119.

(33) Wu, C.; Cheng, D.; Wang, M.; Ma, D. Understanding and Application of Strong Metal-Support Interactions in Conversion of CO2to Methanol: A Review. *Energy Fuels* **2021**, *35* (23), 19012−19023.

(34) Zachopoulos, A.; Heracleous, E. Overcoming the Equilibrium Barriers of CO2 Hydrogenation to Methanol via Water Sorption: A Thermodynamic Analysis. *J. CO2 Util.* **2017**, *21* (May), 360−367.

(35) *CO_2-to-Methanol Plant: Commercial Scale Production in China*; CRI (Carbon Recycling International): Kopavogur, Iceland, 2022.

(36) Rui, N.; Wang, Z.; Sun, K.; Ye, J.; Ge, Q.; Liu, C. CO2 Hydrogenation to Methanol over Pd/In2O3: Effects of Pd and Oxygen Vacancy. *Appl. Catal. B* **2017**, *218*, 488−497.

(37) Martin, O.; Martín, A. J.; Mondelli, C.; Mitchell, S.; Segawa, T. F.; Hauert, R.; Drouilly, C.; Curulla-Ferré, D.; Pérez-Ramírez, J.

https://doi.org/10.1021/acs.energyfuels.4c03013
Energy Fuels 2024, 38, 18265−18291

Indium Oxide as a Superior Catalyst for Methanol Synthesis by CO2 Hydrogenation. *Angew. Chemie - Int. Ed.* **2016**, *55* (21), 6261−6265.
(38) Pasupulety, N.; Driss, H.; Alhamed, Y. A.; Alzahrani, A. A.; Daous, M. A.; Petrov, L. Studies on Au/Cu-Zn-Al Catalyst for Methanol Synthesis from CO2. *Appl. Catal. A Gen.* **2015**, *504*, 308−318.
(39) Słoczyński, J.; Grabowski, R.; Kozłowska, A.; Olszewski, P.; Stoch, J.; Skrzypek, J.; Lachowska, M. Catalytic Activity of the M/(3ZnO·ZrO2) System (M = Cu, Ag, Au) in the Hydrogenation of CO2 to Methanol. *Appl. Catal. A Gen.* **2004**, *278* (1), 11−23.
(40) Sun, K.; Fan, Z.; Ye, J.; Yan, J.; Ge, Q.; Li, Y.; He, W.; Yang, W.; Liu, C. J. Hydrogenation of CO2 to Methanol over In2O3 Catalyst. *J. CO2 Util.* **2015**, *12*, 1−6.
(41) Rui, N.; Zhang, F.; Sun, K.; Liu, Z.; Xu, W.; Stavitski, E.; Senanayake, S. D.; Rodriguez, J. A.; Liu, C. J. Hydrogenation of CO2to Methanol on a Au*δ*+-In2O3- XCatalyst. *ACS Catal.* **2020**, *10* (19), 11307−11317.
(42) Cai, D.; Cai, Y.; Tan, K. B.; Zhan, G. Recent Advances of Indium Oxide-Based Catalysts for CO2 Hydrogenation to Methanol: Experimental and Theoretical. *Materials (Basel)* **2023**, *16* (7), 2803.
(43) Wang, J.; Li, G.; Li, Z.; Tang, C.; Feng, Z.; An, H.; Liu, H.; Liu, T.; Li, C. A Highly Selective and Stable ZnO-ZrO2 Solid Solution Catalyst for CO2 Hydrogenation to Methanol. *Sci. Adv.* **2017**, *3* (10), 1−11.
(44) Wang, X.; Zeng, C. Y.; Gong, N.; Zhang, T.; Wu, Y.; Zhang, J.; Song, F.; Yang, G.; Tan, Y. Effective Suppression of CO Selectivity for CO2Hydrogenation to High-Quality Gasoline. *ACS Catal.* **2021**, *11* (3), 1528−1547.
(45) Men, Y. L.; Liu, Y.; Wang, Q.; Luo, Z. H.; Shao, S.; Li, Y. B.; Pan, Y. X. Highly Dispersed Pt-Based Catalysts for Selective CO2 Hydrogenation to Methanol at Atmospheric Pressure. *Chem. Eng. Sci.* **2019**, *200*, 167−175.
(46) Xiong, S.; Lu, Z.; Shen, C.; Liu, C. ZrO_2 Promoted Ru/In_2O_3 Catalyst for Selective Hydrogenation of CO_2 to Methanol. *Chem. Eng. Sci.* **2023**, *282*, No. 119246.
(47) Zhang, H.; Chen, J.; Han, X.; Pan, Y.; Hao, Z.; Tang, S.; Zi, X.; Zhang, Z.; Gao, P.; Li, M.; Lv, J.; Ma, X. High-Performance Cu/ZnO/Al_2O_3 Catalysts for CO_2 Hydrogenation to Methanol. *Ind. Eng. Chem. Res.* **2024**, *63*, 6210−6221.
(48) Ye, R. P.; Ding, J.; Gong, W.; Argyle, M. D.; Zhong, Q.; Wang, Y.; Russell, C. K.; Xu, Z.; Russell, A. G.; Li, Q.; Fan, M.; Yao, Y. G. CO_2 Hydrogenation to High-Value Products via Heterogeneous Catalysis. *Nat. Commun.* **2019**, *10* (1), 5698.
(49) Zhao, F.; Fan, L.; Xu, K.; Hua, D.; Zhan, G.; Zhou, S. Hierarchical Sheet-like Cu/Zn/Al Nanocatalysts Derived from LDH/MOF Composites for CO 2 Hydrogenation to Methanol. *J. CO2 Util.* **2019**, *33* (March), 222−232.
(50) Cai, Z.; Dai, J.; Li, W.; Tan, K. B.; Huang, Z.; Zhan, G.; Huang, J.; Li, Q. Pd Supported on MIL-68 (In) -Derived In_2O_3 Nanotubes as Superior Catalysts to Boost CO_2 Hydrogenation to Methanol. *ACS Catal.* **2020**, *10*, 13275−13289.
(51) Cai, Y.; Lin, C.; Cha, X.; Wu, Y.; Rao, X.; Tan, K. B.; Cai, D.; Zhuang, G.; Zhan, G. Antiover-Reduction of Ni/In_2O_3 Nanocatalysts by Atomic Layer Deposition of Al_2O_3 Films for Durable CO_2 Hydrogenation to Methanol. *ACS Catal.* **2024**, *14*, 8463−8479.
(52) Li, W.; Wang, K.; Huang, J.; Liu, X.; Fu, D.; Huang, J.; Li, Q.; Zhan, G. M_xO_y−ZrO_2 (M = Zn, Co, Cu) Solid Solutions Derived from Schiff Base-Bridged UiO-66 Composites as High-Performance Catalysts for CO_2 Hydrogenation. *ACS Appl. Mater. Interfaces* **2019**, *11*, 33263−33272.
(53) Li, C.; Yuan, X.; Fujimoto, K. Development of Highly Stable Catalyst for Methanol Synthesis from Carbon Dioxide. *Appl. Catal. A Gen.* **2014**, *469*, 306−311.
(54) Zhang, L.; Liu, X.; Wang, H.; Cao, L.; Huang, C.; Li, S.; Zhang, X.; Guan, Q.; Shao, X.; Lu, J. Size-Dependent Strong Metal-Support Interaction in Pd/ZnO Catalysts for Hydrogenation of CO2to Methanol. *Catal. Sci. Technol.* **2021**, *11* (13), 4398−4405.
(55) Pinheiro Araújo, T.; Mondelli, C.; Agrachev, M.; Zou, T.; Willi, P. O.; Engel, K. M.; Grass, R. N.; Stark, W. J.; Safonova, O. V.; Jeschke, G.; Mitchell, S.; Pérez-Ramírez, J. Flame-Made Ternary Pd-In2O3-ZrO2 Catalyst with Enhanced Oxygen Vacancy Generation for CO2 Hydrogenation to Methanol. *Nat. Commun.* **2022**, *13* (1), 1−12.
(56) Wu, C.; Lin, L.; Liu, J.; Zhang, J.; Zhang, F.; Zhou, T.; Rui, N.; Yao, S.; Deng, Y.; Yang, F.; Xu, W.; Luo, J.; Zhao, Y.; Yan, B.; Wen, X. D.; Rodriguez, J. A.; Ma, D. Inverse ZrO_2/Cu as a Highly Efficient Methanol Synthesis Catalyst from CO_2 Hydrogenation. *Nat. Commun.* **2020**, *11* (1), 5767.
(57) Fujitani, T.; Saito, M.; Kanai, Y.; Watanabe, T.; Nakamura, J.; Uchijima, T. Development of an Active Ga2O3 Supported Palladium Catalyst for the Synthesis of Methanol from Carbon Dioxide and Hydrogen. *Appl. Catal. A,* **1995**, *125* (2), L199−L202.
(58) Fan, L.; Fujimoto, K. Development of an Active and Stable Ceria-Supported Palladium Catalyst for Hydrogenation of Carbon Dioxide to Methanol. *Appl. Catal. A* **1993**, *106* (1), L1−L7.
(59) Yan, Y.; Wong, R. J.; Ma, Z.; Donat, F.; Xi, S.; Saqline, S.; Fan, Q.; Du, Y.; Borgna, A.; He, Q.; Müller, C. R.; Chen, W.; Lapkin, A. A.; Liu, W. CO2 Hydrogenation to Methanol on Tungsten-Doped Cu/CeO2 Catalysts. *Appl. Catal. B* **2022**, *306*, No. 121098.
(60) Zhou, C.; Shi, J.; Zhou, W.; Cheng, K.; Zhang, Q.; Kang, J.; Wang, Y. Highly Active ZnO-ZrO2 Aerogels Integrated with H-ZSM-5 for Aromatics Synthesis from Carbon Dioxide. *ACS Catal.* **2020**, *10* (1), 302−310.
(61) Ye, J.; Liu, C.; Mei, D.; Ge, Q. Active Oxygen Vacancy Site for Methanol Synthesis from CO_2 Hydrogenation on In_2O_3 (110): A DFT Study. *ACS Catal.* **2013**, *3*, 1296−1306.
(62) Meunier, F. C. Hydrogenation of CO and CO2: Contributions of IR Operando Studies. *Catal. Today* **2023**, *423*, No. 113863.
(63) Li, Z.; Qu, Y.; Wang, J.; Liu, H.; Li, M.; Miao, S.; Li, C. Highly Selective Conversion of Carbon Dioxide to Aromatics over Tandem Catalysts. *Joule* **2019**, *3* (2), 570−583.
(64) Chernyak, S. A.; Corda, M.; Dath, J. P.; Ordomsky, V. V.; Khodakov, A. Y. Light Olefin Synthesis from a Diversity of Renewable and Fossil Feedstocks: State-of the-Art and Outlook. *Chem. Soc. Rev.* **2022**, *51* (18), 7994−8044.
(65) Gao, P.; Li, S.; Bu, X.; Dang, S.; Liu, Z.; Wang, H.; Zhong, L.; Qiu, M.; Yang, C.; Cai, J.; Wei, W.; Sun, Y. Direct Conversion of CO2 into Liquid Fuels with High Selectivity over a Bifunctional Catalyst. *Nat. Chem.* **2017**, *9* (10), 1019−1024.
(66) Lam, E.; Larmier, K.; Tada, S.; Wolf, P.; Safonova, O. V.; Copéret, C. Zr(IV) Surface Sites Determine CH3OH Formation Rate on Cu/ZrO2/SiO2 - CO2 Hydrogenation Catalysts. *Chin. J. Catal.* **2019**, *40* (11), 1741−1748.
(67) Song, G.; Li, M.; Yan, P.; Nawaz, M. A.; Liu, D. High Conversion to Aromatics via CO2-FT over a CO-Reduced Cu-Fe2O3Catalyst Integrated with HZSM-5. *ACS Catal.* **2020**, *10* (19), 11268−11279.
(68) Wang, Y.; Tan, L.; Tan, M.; Zhang, P.; Fang, Y.; Yoneyama, Y.; Yang, G.; Tsubaki, N. Rationally Designing Bifunctional Catalysts as an Efficient Strategy to Boost CO 2 Hydrogenation Producing Value-Added Aromatics. *ACS Catal.* **2019**, *9* (2), 895−901.
(69) Ni, Y.; Chen, Z.; Fu, Y.; Liu, Y.; Zhu, W.; Liu, Z. Selective Conversion of CO2 and H2 into Aromatics. *Nat. Commun.* **2018**, *9* (1), 1−7.
(70) Zhang, J.; Zhang, M.; Chen, S.; Wang, X.; Zhou, Z.; Wu, Y.; Zhang, T.; Yang, G.; Han, Y.; Tan, Y. Hydrogenation of CO2 into Aromatics over a ZnCrO: X-Zeolite Composite Catalyst. *Chem. Commun.* **2019**, *55* (7), 973−976.
(71) Kattel, S.; Yan, B.; Yang, Y.; Chen, J. G.; Liu, P. Optimizing Binding Energies of Key Intermediates for CO2 Hydrogenation to Methanol over Oxide-Supported Copper. *J. Am. Chem. Soc.* **2016**, *138* (38), 12440−12450.
(72) Wang, T.; Yang, C.; Gao, P.; Zhou, S.; Li, S.; Wang, H.; Sun, Y. ZnZrOx Integrated with Chain-like Nanocrystal HZSM-5 as Efficient Catalysts for Aromatics Synthesis from CO2 Hydrogenation. *Appl. Catal. B* **2021**, *286*, No. 119929.
(73) Tan, K. B.; Xu, K.; Cai, D.; Huang, J.; Zhan, G. Rational Design of Bifunctional Catalysts with Proper Integration Manners for CO and

CO2 Hydrogenation into Value-Added Products: A Review. *Chem. Eng. J.* **2023**, *463* (March), No. 142262.
(74) Li, W.; Wang, K.; Zhan, G.; Huang, J.; Li, Q. Hydrogenation of CO2to Dimethyl Ether over Tandem Catalysts Based on Biotemplated Hierarchical ZSM-5 and Pd/ZnO. *ACS Sustain. Chem. Eng.* **2020**, *8* (37), 14058−14070.
(75) Raslavičius, L.; Keršys, A.; Mockus, S.; Keršiene, N.; Starevičius, M. Liquefied Petroleum Gas (LPG) as a Medium-Term Option in the Transition to Sustainable Fuels and Transport. *Renew. Sustain. Energy Rev.* **2014**, *32*, 513−525.
(76) Chung, K. H.; Xu, C.; Saito, I.; Laureshen, C. Preface. *Petroleum Science and Technology*; Taylor & Francis, 2006; Vol. *24*, pp 251−252. DOI: 10.1080/10916460500501083.
(77) IARC Working Group on the Evaluation of Carcinogenic Risks to Humans. Occupational Exposures in Petroleum Refining; Crude on and Major Petroleum Fuels. *IARC Monographs on the Evaluation of Carcinogenic Risks to Humans*, Vol. *45*; International Agency for Research on Cancer (IARC), 1988; p 331.
(78) Chen, F.; Satizabal, V. Presentation: Fluidized bed Methanol to Gasoline (MTG): A Reliable and Cost-Effective Solution for Production of Renewable Gasoline. *ExxonMobil Library*; ExxonMobil, 2021. https://www.exxonmobilchemical.com/en/resources/library/library-detail/87913/mtg_afpm_fengrong_and_victoria_recorded_oct_2021.
(79) Arias Gallego, C.; Khandavilli, M.; Kobayashi, L.; Sarathy, S. M. Kinetic Modeling and Techno-Economic Analysis of a Methanol-to-Gasoline Production Repurposed Refinery Equipment. *ACS Omega* **2024**, *9* (21), 22858−22870.
(80) Amaral, L. V.; Santos, N. D. S. A.; Roso, V. R.; Sebastiao, R. d. C. d. O.; Pujatti, F. J. P. Effects of Gasoline Composition on Engine Performance, Exhaust Gases and Operational Costs. *Renewable Sustainable Energy Rev.* **2021**, *135*, 110196.
(81) Badia, J. H.; Ramírez, E.; Bringué, R.; Cunill, F.; Delgado, J. New Octane Booster Molecules for Modern Gasoline Composition. *Energy Fuels* **2021**, *35* (14), 10949−10997.
(82) Gogate, M. R. Methanol-to-Olefins Process Technology: Current Status and Future Prospects. *Pet. Sci. Technol.* **2019**, *37* (5), 559−565.
(83) Hindman, M. L. Methanol to Gasoline Technology. *Proceedings of the Twenty-Third (2013) International Offshore and Polar Engineering Conference*; International Society of Offshore and Polar Engineers (ISOPE), 2013; pp 38−41.
(84) Tan, K. B.; Zhan, G.; Sun, D.; Huang, J.; Li, Q. The Development of Bifunctional Catalysts for Carbon Dioxide Hydrogenation to Hydrocarbonsviathe Methanol Route: From Single Component to Integrated Components. *J. Mater. Chem. A* **2021**, *9* (9), 5197−5231.
(85) Li, T.; Shoinkhorova, T.; Gascon, J.; Ruiz-Martinez, J. Aromatics Production via Methanol-Mediated Transformation Routes. *ACS Catal.* **2021**, *11* (13), 7780−7819.
(86) Kianfar, E.; Hajimirzaee, S.; mousavian, S.; Mehr, A. S. Zeolite-Based Catalysts for Methanol to Gasoline Process: A Review. *Microchem. J.* **2020**, *156*, No. 104822.
(87) Schulz, H. Coking" of Zeolites during Methanol Conversion: Basic Reactions of the MTO-, MTP- and MTG Processes. *Catal. Today* **2010**, *154* (3−4), 183−194.
(88) Olsbye, U.; Svelle, S.; Bjørgen, M.; Beato, P.; Janssens, T. V. W.; Joensen, F.; Bordiga, S.; Lillerud, K. P. Conversion of Methanol to Hydrocarbons: How Zeolite Cavity and Pore Size Controls Product Selectivity. *Angew. Chem., Int. Ed.* **2012**, *51* (24), 5810−5831.
(89) Gayubo, A. G.; Aguayo, A. T.; Morán, A. L.; Olazar, M.; Bilbao, J. Role of Water in the Kinetic Modeling of Catalyst Deactivation in the MTG Process. *AIChE J.* **2002**, *48* (7), 1561−1571.
(90) Arora, S. S.; Nieskens, D. L. S.; Malek, A.; Bhan, A. Lifetime Improvement in Methanol-to-Olefins Catalysis over Chabazite Materials by High-Pressure H2 Co-Feeds. *Nat. Catal.* **2018**, *1* (9), 666−672.
(91) Martín, N.; Portillo, A.; Ateka, A.; Cirujano, F. G.; Oar-Arteta, L.; Aguayo, A. T.; Dusselier, M. MOF-Derived/Zeolite Hybrid Catalyst for the Production of Light Olefins from CO2. *ChemCatChem.* **2020**, *12* (22), 5750−5758.
(92) Haw, J. F.; Song, W.; Marcus, D. M.; Nicholas, J. B. The Mechanism of Methanol to Hydrocarbon Catalysis. *Acc. Chem. Res.* **2003**, *36* (5), 317−326.
(93) Zhang, X.; Zhang, A.; Jiang, X.; Zhu, J.; Liu, J.; Li, J.; Zhang, G.; Song, C.; Guo, X. Utilization of CO2 for Aromatics Production over ZnO/ZrO2-ZSM-5 Tandem Catalyst. *J. CO2 Util.* **2019**, *29*, 140−145.
(94) Shah, D. R.; Nezam, I.; Zhou, W.; Proaño, L.; Jones, C. W. Isomorphous Substitution in ZSM-5 in Tandem Methanol/Zeolite Catalysts for the Hydrogenation of CO2 to Aromatics. *Energy Fuels* **2024**, *38*, 2224−2234.
(95) Ni, X.; Tan, Y.; Han, Y.; Tsubaki, N. Synthesis of Isoalkanes over Fe-Zn-Zr/HY Composite Catalyst through Carbon Dioxide Hydrogenation. *Catal. Commun.* **2007**, *8* (11), 1711−1714.
(96) Wang, X.; Yang, G.; Zhang, J.; Chen, S.; Wu, Y.; Zhang, Q.; Wang, J.; Han, Y.; Tan, Y. Synthesis of Isoalkanes over a Core (Fe-Zn-Zr)-Shell (Zeolite) Catalyst by CO2 Hydrogenation. *Chem. Commun.* **2016**, *52* (46), 7352−7355.
(97) Wang, Y.; Gao, W.; Kazumi, S.; Li, H.; Yang, G.; Tsubaki, N. Direct and Oriented Conversion of CO_2 into Value-Added Aromatics. *Chem. - A Eur. J.* **2019**, *25* (20), 5149−5153.
(98) Dokania, A.; Ould-Chikh, S.; Ramirez, A.; Cerrillo, J. L.; Aguilar, A.; Russkikh, A.; Alkhalaf, A.; Hita, I.; Bavykina, A.; Shterk, G.; Wehbe, N.; Prat, A.; Lahera, E.; Castaño, P.; Fonda, E.; Hazemann, J.-L.; Gascon, J. Designing a Multifunctional Catalyst for the Direct Production of Gasoline-Range Isoparaffins from CO 2. *JACS Au* **2021**, *1* (11), 1961−1974.
(99) Rigamonti, M. G.; Shah, M.; Gambu, T. G.; Saeys, M.; Dusselier, M. Reshaping the Role of CO2in Propane Dehydrogenation: From Waste Gas to Platform Chemical. *ACS Catal.* **2022**, *12* (15), 9339−9358.
(100) Bavykina, A.; Yarulina, I.; Al Abdulghani, A. J.; Gevers, L.; Hedhili, M. N.; Miao, X.; Galilea, A. R.; Pustovarenko, A.; Dikhtiarenko, A.; Cadiau, A.; Aguilar-Tapia, A.; Hazemann, J. L.; Kozlov, S. M.; Oud-Chikh, S.; Cavallo, L.; Gascon, J. Turning a Methanation Co Catalyst into an In-Co Methanol Producer. *ACS Catal.* **2019**, *9* (8), 6910−6918.
(101) Ronda-Lloret, M.; Rothenberg, G.; Shiju, N. R. A Critical Look at Direct Catalytic Hydrogenation of Carbon Dioxide to Olefins. *ChemSusChem* **2019**, *12* (17), 3896−3914.
(102) Coffano, C.; Porta, A.; Visconti, C. G.; Rabino, F.; Franzoni, G.; Picutti, B.; Lietti, L. One-Pot Lower Olefins Production from CO2 Hydrogenation. *Catal. Today* **2023**, *418*, No. 114133.
(103) Ramirez, A.; Gong, X.; Caglayan, M.; Nastase, S. A. F.; Abou-Hamad, E.; Gevers, L.; Cavallo, L.; Dutta Chowdhury, A.; Gascon, J. Selectivity Descriptors for the Direct Hydrogenation of CO2 to Hydrocarbons during Zeolite-Mediated Bifunctional Catalysis. *Nat. Commun.* **2021**, *12* (1), 1−13.
(104) Yue, Y.; Tian, J.; Ma, J.; Yang, S.; Li, W.; Huang, J.; Li, Q.; Zhan, G. Regulation of Acidity Properties of ZSM-5 and Proximity between Metal Oxide and Zeolite on Bifunctional Catalysts for Enhanced CO2 Hydrogenation to Aromatics. *Appl. Catal. B* **2024**, *355*, No. 124158.
(105) Li, W.; Zhan, G.; Liu, X.; Yue, Y.; Tan, K. B.; Wang, J.; Huang, J.; Li, Q. Assembly of ZnZrOx and ZSM-5 on Hierarchically Porous Bio-Derived SiO2 Platform as Bifunctional Catalysts for CO2 Hydrogenation to Aromatics. *Appl. Catal. B* **2023**, *330*, No. 122575.
(106) Shen, X.; Kang, J.; Niu, W.; Wang, M.; Zhang, Q.; Wang, Y. Impact of Hierarchical Pore Structure on the Catalytic Performances of MFI Zeolites Modified by ZnO for the Conversion of Methanol to Aromatics. *Catal. Sci. Technol.* **2017**, *7* (16), 3598−3612.
(107) Kerstens, D.; De Peuter, H.; Khalil, I.; Van Praet, S.; Van Aelst, J.; Sels, B. F. Fast and Selective Solvent-Free Branching of Unsaturated Fatty Acids with Hierarchical ZSM-5. *ACS Sustain. Chem. Eng.* **2021**, *9* (12), 4357−4362.
(108) Peeters, E.; Khalil, I.; Eloy, P.; Calderon-Ardila, S.; Dijkmans, J.; Ferrini, P.; Debecker, D. P.; Taylor, R. A.; Douvalis, A. P.;

Dusselier, M.; Sels, B. F. Tandem Reduction-Reoxidation Augments the Catalytic Activity of Sn-Beta Zeolites by Redispersion and Respeciation of SnO2Clusters. *Chem. Mater.* **2021**, *33* (23), 9366−9381.
(109) Thibault-Starzyk, F.; Stan, I.; Abelló, S.; Bonilla, A.; Thomas, K.; Fernandez, C.; Gilson, J. P.; Pérez-Ramírez, J. Quantification of Enhanced Acid Site Accessibility in Hierarchical Zeolites - The Accessibility Index. *J. Catal.* **2009**, *264* (1), 11−14.
(110) Mole, T.; Whiteside, J. A.; Seddon, D. Aromatic Co-Catalysis of Methanol Conversion over Zeolite Catalysts. *J. Catal.* **1983**, *82* (2), 261−266.
(111) Ilias, S.; Bhan, A. The Mechanism of Aromatic Dealkylation in Methanol-to-Hydrocarbons Conversion on H-ZSM-5: What Are the Aromatic Precursors to Light Olefins? *J. Catal.* **2014**, *311*, 6−16.
(112) Sassi, A.; Wildman, M. A.; Haw, J. F. Reactions of Butylbenzene Isomers on Zeolite Hbeta: Methanol-to-Olefins Hydrocarbon Pool Chemistry and Secondary Reactions of Olefins. *J. Phys. Chem. B* **2002**, *106* (34), 8768−8773.
(113) Wang, X.; Yang, G.; Zhang, J.; Song, F.; Wu, Y.; Zhang, T.; Zhang, Q.; Tsubaki, N.; Tan, Y. Macroscopic Assembly Style of Catalysts Significantly Determining Their Efficiency for Converting CO2 to Gasoline. *Catal. Sci. Technol.* **2019**, *9* (19), 5401−5412.
(114) Kim, J.; Choi, M.; Ryoo, R. Effect of Mesoporosity against the Deactivation of MFI Zeolite Catalyst during the Methanol-to-Hydrocarbon Conversion Process. *J. Catal.* **2010**, *269* (1), 219−228.
(115) Rodemerck, U.; Holeňa, M.; Wagner, E.; Smejkal, Q.; Barkschat, A.; Baerns, M. Catalyst Development for CO2 Hydrogenation to Fuels. *ChemCatChem.* **2013**, *5* (7), 1948−1955.
(116) Dorner, R. W.; Hardy, D. R.; Williams, F. W.; Willauer, H. D. Heterogeneous Catalytic CO2 Conversion to Value-Added Hydrocarbons. *Energy Environ. Sci.* **2010**, *3* (7), 884−890.
(117) Scarfiello, C.; Soulantica, K.; Cayez, S.; Durupt, A.; Viau, G.; Le Breton, N.; Boudalis, A. K.; Meunier, F.; Clet, G.; Barreau, M.; Salusso, D.; Zafeiratos, S.; Minh, D. P.; Serp, P. Modified Co/TiO_2 Catalysts for CO_2 Hydrogenation to Fuels. *J. Catal.* **2023**, *428*, 115202.
(118) Chernyak, S. A.; Corda, M.; Marinova, M.; Safonova, O. V.; Kondratenko, V. A.; Kondratenko, E. V.; Kolyagin, Y. G.; Cheng, K.; Ordomsky, V. V.; Khodakov, A. Y. Decisive Influence of SAPO-34 Zeolite on Light Olefin Selectivity in Methanol-Meditated CO2 Hydrogenation over Metal Oxide-Zeolite Catalysts. *ACS Catal.* **2023**, *13* (22), 14627−14638.
(119) Meunier, F. C.; Dansette, I.; Paredes-Nunez, A.; Schuurman, Y. Cu-Bound Formates Are Main Reaction Intermediates during CO2 Hydrogenation to Methanol over Cu/ZrO2. *Angew. Chemie - Int. Ed.* **2023**, *62* (29), 1−6.
(120) Ahmad, M. S.; Cheng, C. K.; Bhuyar, P.; Atabani, A. E.; Pugazhendhi, A.; Chi, N. T. L.; Witoon, T.; Lim, J. W.; Juan, J. C. Effect of Reaction Conditions on the Lifetime of SAPO-34 Catalysts in Methanol to Olefins Process − A Review. *Fuel* **2021**, *283*, 118851.
(121) Graaf, G. H.; Stamhuis, E. J.; Beenackers, A. A. C. M. Kinetics of Low-Pressure Methanol Synthesis. *Chem. Eng. Sci.* **1988**, *43* (12), 3185−3195.
(122) Díez-Ramírez, J.; Díaz, J. A.; Dorado, F.; Sánchez, P. Kinetics of the Hydrogenation of CO2 to Methanol at Atmospheric Pressure Using a Pd-Cu-Zn/SiC Catalyst. *Fuel Process. Technol.* **2018**, *173*, 173−181.
(123) Grabow, L. C.; Mavrikakis, M. Mechanism of Methanol Synthesis on Cu through CO2 and CO Hydrogenation. *ACS Catal.* **2011**, *1* (4), 365−384.
(124) Frei, M. S.; Capdevila-Cortada, M.; García-Muelas, R.; Mondelli, C.; López, N.; Stewart, J. A.; Curulla Ferré, D.; Pérez-Ramírez, J. Mechanism and Microkinetics of Methanol Synthesis via CO2 Hydrogenation on Indium Oxide. *J. Catal.* **2018**, *361*, 313−321.
(125) Huš, M.; Kopač, D.; Štefančič, N. S.; Jurković, D. L.; Dasireddy, V. D. B. C.; Likozar, B. Unravelling the Mechanisms of CO2 Hydrogenation to Methanol on Cu-Based Catalysts Using First-Principles Multiscale Modelling and Experiments. *Catal. Sci. Technol.* **2017**, *7* (24), 5900−5913.
(126) Ghosh, S.; Olsson, L.; Creaser, D. Methanol Mediated Direct CO2 Hydrogenation to Hydrocarbons: Experimental and Kinetic Modeling Study. *Chem. Eng. J.* **2022**, *435* (P3), No. 135090.
(127) Park, T. Y.; Froment, G. F. Kinetic Modeling of the Methanol to Olefins Process. 2. Experimental Results, Model Discrimination, and Parameter Estimation. *Ind. Eng. Chem. Res.* **2001**, *40* (20), 4187−4196.
(128) Kaarsholm, M.; Rafii, B.; Joensen, F.; Cenni, R.; Chaouki, J.; Patience, G. S. Kinetic Modeling of Methanol-to-Olefin Reaction over ZSM-5 in Fluid Bed. *Ind. Eng. Chem. Res.* **2010**, *49* (1), 29−38.
(129) Aguayo, A. T.; Mier, D.; Gayubo, A. G.; Gamero, M.; Bilbao, J. Kinetics of Methanol Transformation into Hydrocarbons on a HZSM-5 Zeolite Catalyst at High Temperature (400−550°c). *Ind. Eng. Chem. Res.* **2010**, *49* (24), 12371−12378.
(130) Kumar, P.; Thybaut, J. W.; Svelle, S.; Olsbye, U.; Marin, G. B. Single-Event Microkinetics for Methanol to Olefins on H-ZSM-5. *Ind. Eng. Chem. Res.* **2013**, *52* (4), 1491−1507.
(131) Lee, M. K.; Kim, J.; Ryu, J. H.; Yoon, Y. S.; Kim, C. U.; Jeong, S. Y.; Lee, I. B. Modeling of Reaction and Deactivation Kinetics in Methanol-to-Olefins Reaction on SAPO-34. *Ind. Eng. Chem. Res.* **2019**, *58* (29), 13227−13238.
(132) Cordero-Lanzac, T.; Ramirez, A.; Cruz-Fernandez, M.; Zander, H. J.; Joensen, F.; Woolass, S.; Meiswinkel, A.; Styring, P.; Gascon, J.; Olsbye, U. A CO_2 valorization Plant to Produce Light Hydrocarbons: Kinetic Model, Process Design and Life Cycle Assessment. *J. CO2 Util.* **2023**, *67*, 102337.
(133) Pérez-Uriarte, P.; Ateka, A.; Aguayo, A. T.; Gayubo, A. G.; Bilbao, J. Kinetic Model for the Reaction of DME to Olefins over a HZSM-5 Zeolite Catalyst. *Chem. Eng. J.* **2016**, *302*, 801−810.
(134) Ghosh, S.; Sebastian, J.; Olsson, L.; Creaser, D. Experimental and Kinetic Modeling Studies of Methanol Synthesis from CO2 Hydrogenation Using In2O3 Catalyst. *Chem. Eng. J.* **2021**, *416*, No. 129120.
(135) Skov; Ridjan, I. A.; Hamza. *Renewable Aviation e-SAF Catalogue and System Impacts*; Aalborg University, 2024.

https://doi.org/10.1021/acs.energyfuels.4c03013
Energy Fuels 2024, 38, 18265−18291